Effect of insoluble materials on the volumetric behavior of rock salt

Mejda Azabou, Ahmed Rouabhi, Laura Blanco Martín

Version of Record: https://www.sciencedirect.com/science/article/pii/S1674775520301232
Manuscript_fcc8a26e2d39f750014245c232488293

Effect of insoluble materials on the volumetric behavior of rock salt

M. Azabou[a,*], A. Rouabhi[a], L. Blanco-Martín[a]

[a]*MINES ParisTech, PSL Research University, Centre de Géosciences, 35 rue St Honoré 77300 Fontainebleau, France*

Abstract

This paper focuses on the presence of nodules of insoluble materials within salt specimens, and their effect on the volumetric strain measurements and the dilatancy phenomenon. We analyzed experimental results of over 120 conventional triaxial compression tests, and found that in 20% of the cases the volumetric strain measurements were atypical. We also noted that the natural variability of the specimens can lead to a non negligible data scattering in the volumetric strain measurements, when different specimens are subjected to the same test. This is expected given the small magnitude of those strains, but it occasionally implies that the corresponding specimens are not representative of the volumetric behavior of the studied rock. In order to understand these results, we conducted numerical investigations in which salt specimens are modeled as halite matrices with inclusions of impurities. Simulations of triaxial compression tests on these structures proved that such heterogeneities can induce dilatancy: their presence led to the appearance of tensile zones which is physically translated into a micro-cracking activity. The modeling approach was validated as the patterns displayed in the numerical results were identical to what is seen in the laboratory. It was then employed to provide an explanation to the observed irregularities in experimental results. We studied the natural variability effect as well and proposed a methodology to overcome the issue of specimens representativity from both deviatoric and volumetric perspectives.

Keywords: rock salt, dilatancy, material heterogeneity, natural variability, triaxial tests, virtual laboratory

1. Introduction

Solution mined cavities in salt formations have been used for hydrocarbon storage for about 70 years (Bays, 1963). What made this technique conceivable in the first place is the excellent sealing capacity of rock salt due to its naturally low porosity and permeability (Popp and Kern, 1998; Wang et al., 2019). However, underground cavity opening in undisturbed rocks results in the creation of disturbed zones around the underground facility (DeVries et al., 2002, 2005; Habibi, 2019), where the stress state is far from being isotropic and can present high levels of deviatoric stress (DeVries et al., 2002; Tsang et al., 2005).

Laboratory tests on salt specimens have proven that, under compressive loading and above some level of deviatoric stress, rock salt can undergo an irreversible volume increase resulting from a micro-cracking activity (DeVries et al., 2005). This phenomenon is known as dilatancy and is associated with material damage since the micro-cracking activity weakens the material and allows the development of flow paths (Stormont, 1997; Schulze et al., 2001; DeVries et al., 2002). Figure 1 shows the dilatancy onset during a triaxial test conducted under a confining pressure of 4 MPa and a constant axial strain rate of 5×10^{-5} s^{-1}.

*Corresponding author
Email address: mejda.azabou@mines-paristech.fr (M. Azabou)

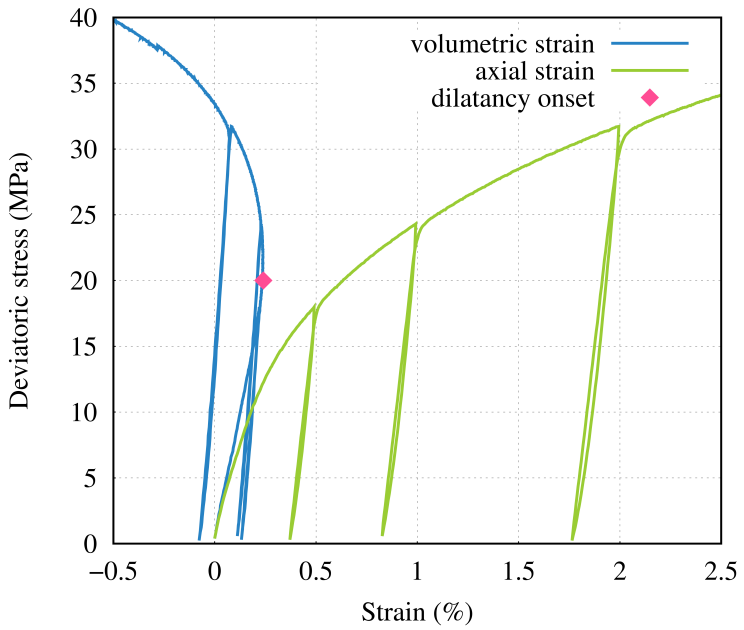

Figure 1: Experimental data of a triaxial compression test on a rock salt specimen (test conducted at Mines ParisTech). Compressive strains are positive.

Due to the stress state distribution around the cavity, dilatancy is likely to occur, compromising the integrity of the facility (DeVries et al., 2002; Wang et al., 2018; Labaune, 2018), hence the importance of the experimental measurements of volumetric strain. However, rock salt dilatancy usually occurs at small volumetric strains (typically below 0.4% (Roberts et al., 2015; Labaune, 2018; Rouabhi et al., 2019)), which is so small that rock salt viscoplastic deformation was considered isochoric for years (Munson and Dawson, 1981; Tijani et al., 1983; Heusermann et al., 2003). Thus, getting the accurate data is a delicate task as factors like natural variability, specimen heterogeneity, testing procedure or the used measurement techniques can significantly impact the results. Studies on factors influencing the volumetric strain measurements have been carried out: Medina-Cetina and Rechenmacher (2009); DeVries and Mellegard (2010) investigated the effect of specimens preconditioning; Hou (2003); DeVries et al. (2005); Rouabhi et al. (2019) tackled the effect of aspects of the loading conditions, and the measurement techniques effect was studied in Rouabhi et al. (2019).

Natural variability is an inevitable bias since we are studying a geological material. As will be

shown throughout this paper, the natural variability of the specimens has a slight effect on the deviatoric behavior; the exhibited dispersion in axial strain measurements remains within the ranges of measurements errors. However, regarding the volumetric ones, and due to their small magnitude as already mentioned, the measured volumetric behavior can show a non negligible dispersion. And this means that the used specimens could be non representative of the corresponding rock salt on the volumetric level albeit they are so from a deviatoric point of view.

The work of Rouabhi et al. (2019) and further illustrations throughout this paper show that if we exclude the dysfunction of the measurement techniques, volumetric strain data given by different measurement techniques can exhibit differences that cannot be attributed to the testing conditions alone. This raises questions concerning the material heterogeneity as it can lead to spatial heterogeneities in the stress and strain fields.

There are numerous aspects of material heterogeneity, they can be microscopic, i.e., related to the shape, size and orientation of the grains, related to fluid inclusions in grain boundaries or to the type of halite crystals (see Chemin, 1990; Van-Hasselt, 1991; Speranza et al., 2016, and references therein), as they can be macroscopic and visible on the specimen like the presence of nodules of anhydrite or clay, or even fracture plans. More details into the microscopic and macroscopic aspects of natural heterogeneity in rock salt can be found in the work of Speranza et al. (2016) and the references therein. The impurities present in rock salt are usually clay, anhydrite and marl Gillhaus et al. (2006). Their mass fraction is usually determined in the process of site characterization. It is a property that varies from one rock salt to another over a large range: in the Tersanne cavern field in south eastern France, the mass fraction of impurities in the salt formation is less than 10%, while in other formations this fraction can be greater than 50% (the Vauvert cavern field in south France).

To the best of the authors' knowledge, no studies have been carried out to investigate neither the effect of natural variability nor the impact of a specimen's spatial heterogeneity on the volumetric strain measurements, especially since they are used to determine design criteria for salt caverns.

The main purpose of this paper is to understand the effect of material heterogeneity on the experimental measurements of volumetric strain and to propose a methodology to overcome the issue of specimens representativity from a volumetric perspective. We chose to focus our work on the

presence of macroscopic nodules of insoluble materials within a supposedly pure halite matrix. Experimentally, investigating such factors is a delicate task as it requires precise data and cannot tolerate measurement errors and perturbations that are difficult to quantify. For this reason, we support our experimental investigation by an extensive numerical study. The use of a virtual laboratory will allow a better understanding of what is observed in the lab and will offer a ground to investigate the dilatancy phenomenon with a structural approach without the limitations of experimental works.

We mainly found that the dilatancy phenomenon could be a consequence of material heterogeneity and that the presence of insoluble materials can explain some of the atypical observations in the lab. We also showed how sensitive the volumetric strain measurements are to the natural variability of the specimens and proposed a methodology to overcome the issue of non representativity.

This paper is structured as follows. Section 2 is an experimental investigation that is focused on the volumetric strain measurements. Section 3 briefly presents the constitutive model used in the numerical study of section 4 during which the effect of heterogeneities on the volumetric behavior is investigated. This study is purely mechanical, neither the thermal nor the hydraulic aspects were taken into account.

2. Experimental data

We analyzed 11 experimental campaigns conducted at the Geosciences Department of Mines ParisTech on salt specimens from different locations in France and in the US between 2004 and 2012. Each testing program is comprised of conventional uniaxial and triaxial compression tests and creep tests. As volumetric strain measurements are only provided in triaxial compression tests, we focused our analysis on those experiments and the total number of studied tests was about 123. The tested specimens are 13 cm high cylinders with a slenderness ratio of 2. A triaxial compression test consists in maintaining a constant confining pressure on the lateral surface of the specimen by injecting/withdrawing a confining fluid into a triaxial cell, while imposing a constant axial strain rate via loading platens between which the specimen is placed (Wawersik and Hannum, 1980; Mellegard et al., 2005; Ulusay et al., 2007).

We distinguish two kinds of measurement techniques; "local" and "global". The local measure-

ments are given by strain gauges (axial and circumferential) placed at mid height of the specimen. The global measurements use an LVDT (linear variable displacement transducer) sensor attached to the loading platens and the amount of fluid injected or withdrawn from the cell (Rouabhi et al., 2019). Thus for the axial strain, the local measurement is given by the axial strain gauge and the global one is given by the LVDT sensor. The measurements of the axial and circumferential gauges are combined to get the local volumetric strain measurement whereas the axial displacement between the loading platens (measured by the LVDT) is combined with the amount of fluid injected or withdrawn from the cell to get the global volumetric strain measurement.

In the following, let Q be the applied axial stress, P the confining pressure, $|Q - P|$ the deviatoric stress and ζ the volumetric strain defined as:

$$\begin{cases} \zeta_g = -(V - V_i)/V_i \\ \zeta_l = -(2\varepsilon_\theta + \varepsilon_z) \end{cases} \tag{1}$$

where the subscripts g, l and i stand respectively for global, local and initial. The volume of the specimen is V, ε_θ and ε_z are the tangential and axial strains, respectively. Refer to Rouabhi et al. (2019) and references therein for further details on the given definitions.

2.1. Results and observations

The analysis of the experimental data and the examination of the corresponding specimens showed that in about 80% of the tests, the difference between the local and global measurements of axial strain is small and stays within the range of the uncertainty of the measurement techniques. Regarding the volumetric strain, there is always a difference between global and local measurements as the strain gauges measure dilatancy onset before it is seen by the whole specimen, i.e, before the global measurement indicates it. In these classic cases, the dispersion between local and global measurements is in the range of what is seen in the tests presented in the work of Rouabhi et al. (2019). Figure 2 shows the results of a typical test conducted under a constant strain rate of 5×10^{-5} s^{-1} and a confining pressure of 12 MPa. In this figure, the evolution of the deviatoric stress is presented as a function of global and local measurements of the axial and volumetric strains. As it can be seen, the dilatancy onset given by the global technique is about 2 times higher than the

one measured by the gauges, and this is a ratio that is seen in a large majority of the tests. On the other hand, the axial strain measurements present an acceptable dispersion.

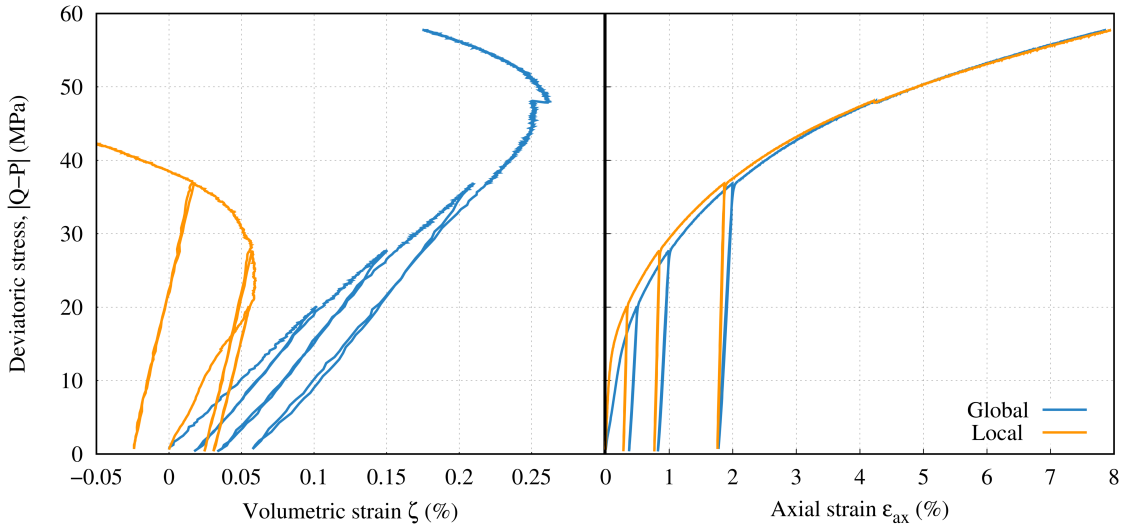

Figure 2: Results of a conventional triaxial compression test (P=12 MPa, $\dot{\varepsilon}_{ax} = 5 \times 10^{-5}$ s^{-1}) representative of 80% of the tests performed.

Regarding the remaining 20% of the tests, the local volumetric strain measurements are atypical and their comparison with the global ones is out of the pattern described for 80% of the tests. In these tests, we have cases where gauges indicate a higher deviatoric stress for dilatancy onset than what the global technique indicates. We also see cases where the gauges measure only contractancy or dilatancy during the entire test period whereas the global technique shows that the specimen undergoes contractancy and then dilatancy. Figures 3 to 6 give examples of these atypical observations and show the corresponding specimens as well. In Figure 3 the deviatoric stress corresponding to the global dilatancy onset is 8 times higher than the one measured by the local technique. Figure 4 indicates that when the deviatoric stress ranges between 35 and 50 MPa, the specimen undergoes a global increase in volume and a local contractancy at the same time. Figures 5 and 6 show that the local and global volumetric behaviors are significantly different during each of these tests.

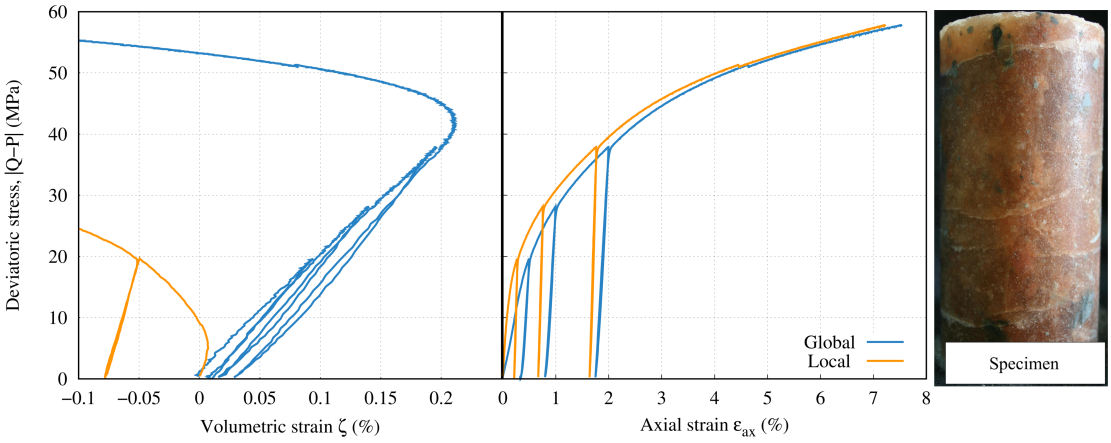

Figure 3: Results of a triaxial compression test (P= 12 MPa, $\dot{\varepsilon}_{ax} = 5 \times 10^{-5}$ s^{-1}) and the corresponding tested salt specimen, an example of the irregularities observed in 20% of the performed tests.

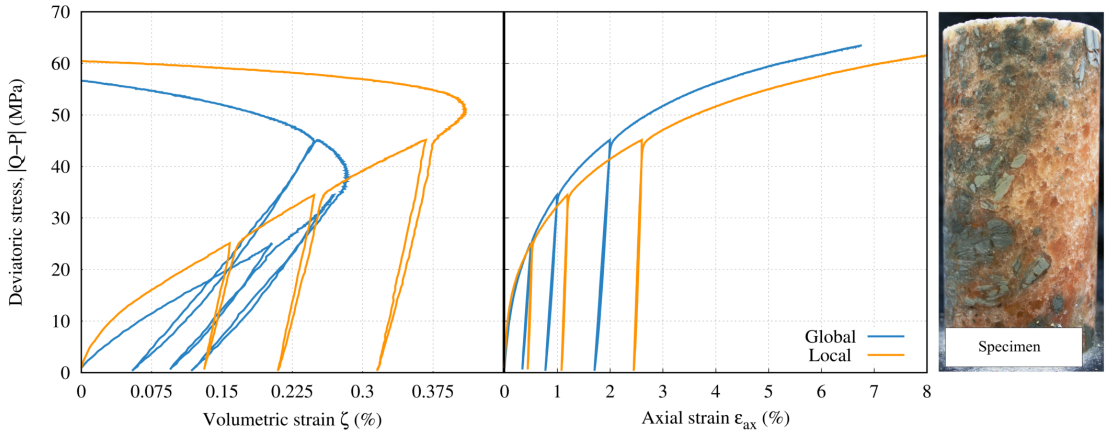

Figure 4: Results of a triaxial compression test (P= 12 MPa, $\dot{\varepsilon}_{ax} = 5 \times 10^{-5}$ s^{-1}) and the corresponding tested salt specimen, an example of the irregularities observed in 20% of the performed tests.

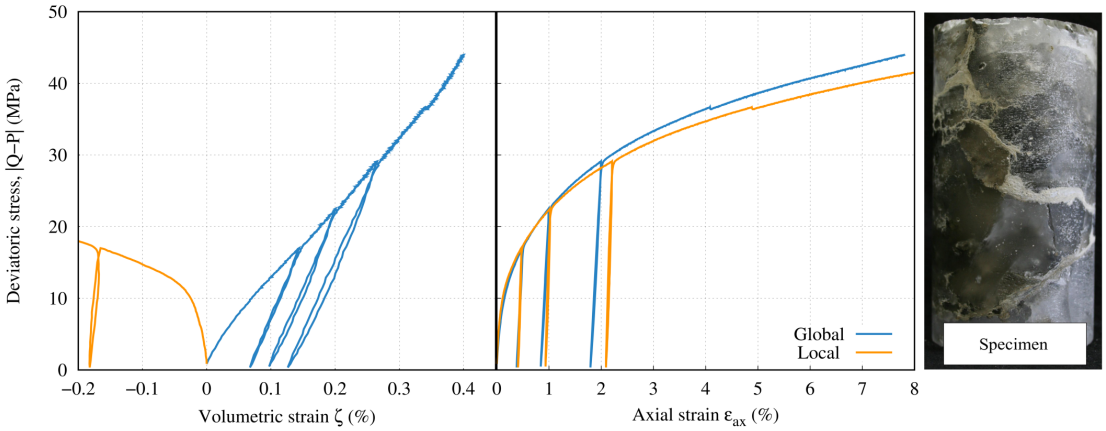

Figure 5: Results of a triaxial compression test (P= 12 MPa, $\dot{\varepsilon}_{ax} = 5 \times 10^{-5}$ s^{-1}) and the corresponding tested salt specimen, an example of the irregularities observed in 20% of the performed tests.

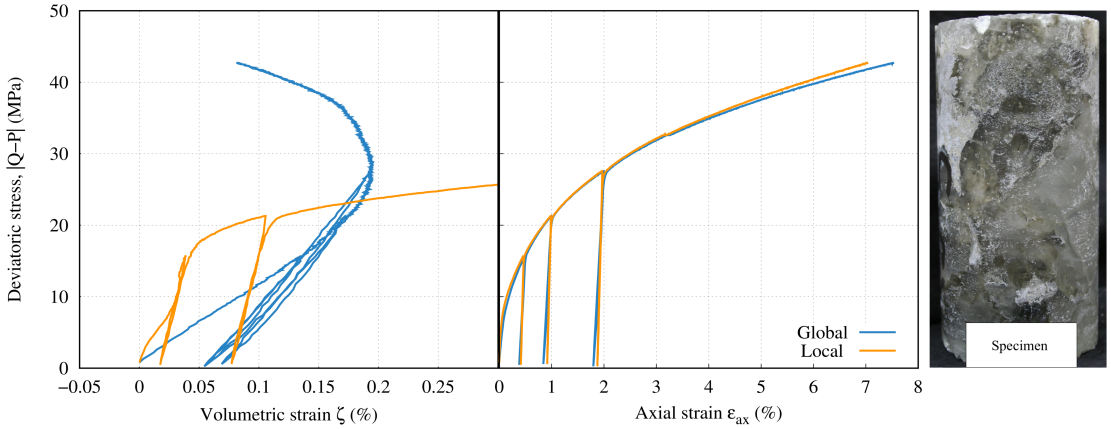

Figure 6: Results of a triaxial compression test (P= 8 MPa, $\dot{\varepsilon}_{ax} = 5 \times 10^{-5}$ s^{-1}) and the corresponding tested salt specimen, an example of the irregularities observed in 20% of the performed tests.

We have also studied the cases where the same test is conducted on two specimens in order to see to which extent could the natural variability affect the results and whether the resulting dispersion is acceptable. We observed that the natural variability does not have a significant effect on the axial strain, be it local or global, but it could significantly affect the volumetric behavior measurements. In Figures 7 to 9, we show 3 of these comparisons along with the concerned specimens.

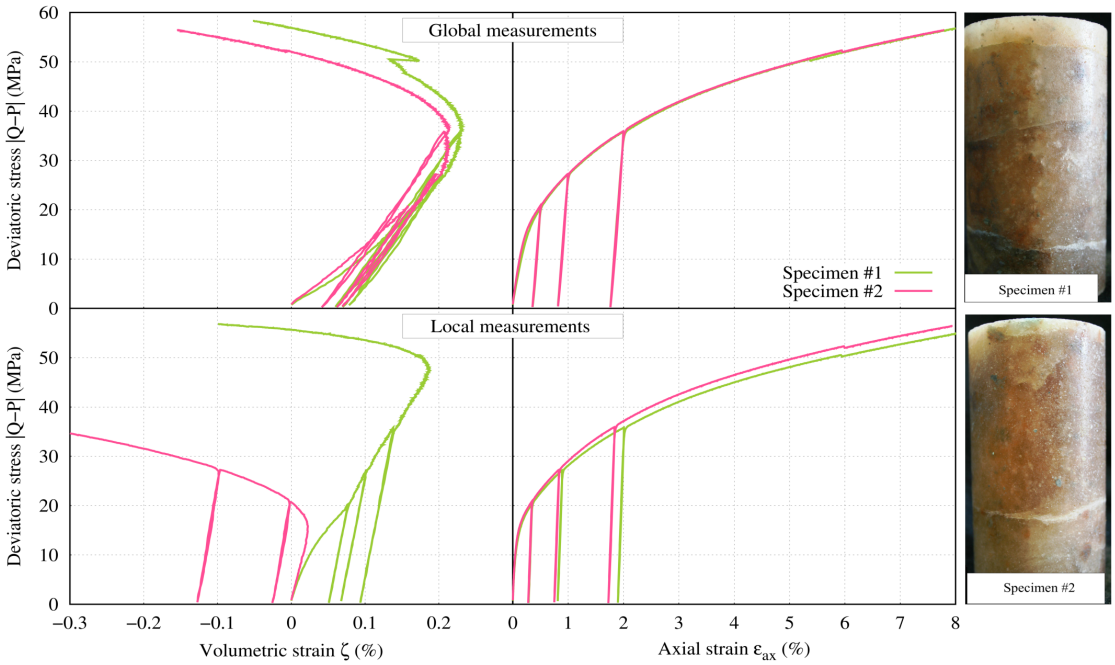

Figure 7: Results of two identical triaxial compression tests (P= 8 MPa, $\dot{\varepsilon}_{ax} = 5 \times 10^{-5}$ s^{-1}) and the corresponding tested salt specimens with difference in depths of 2.25 m.

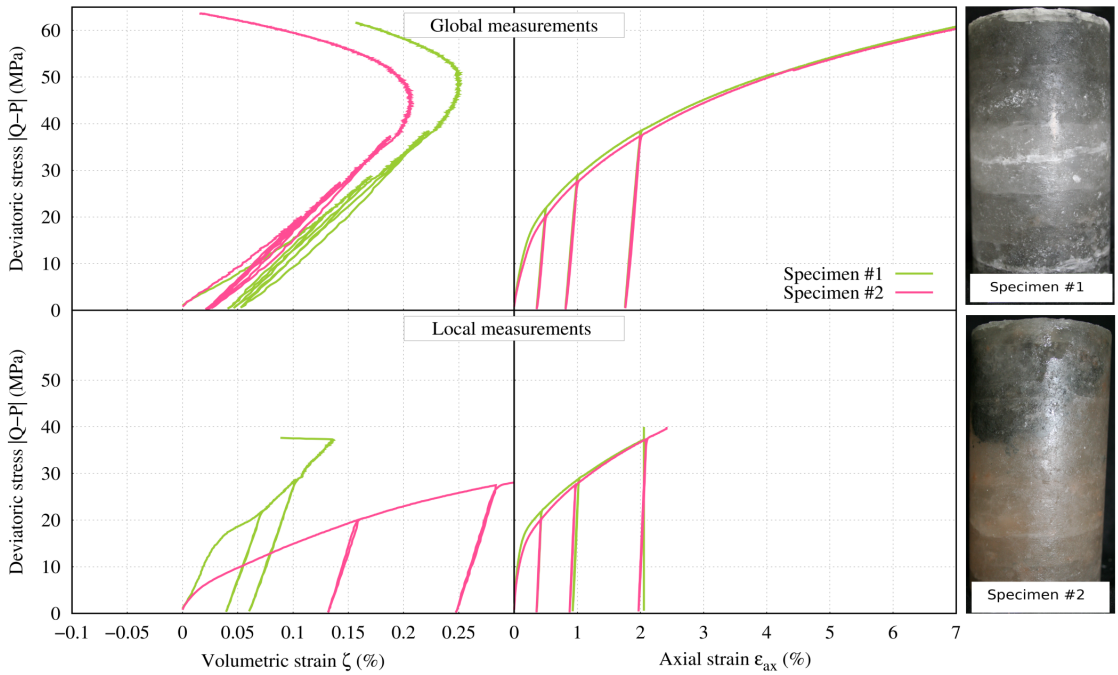

Figure 8: Results of two identical triaxial compression tests (P= 12 MPa, $\dot{\varepsilon}_{ax} = 5 \times 10^{-5}$ s^{-1}) and the corresponding tested salt specimens with difference in depths of 2.3 m.

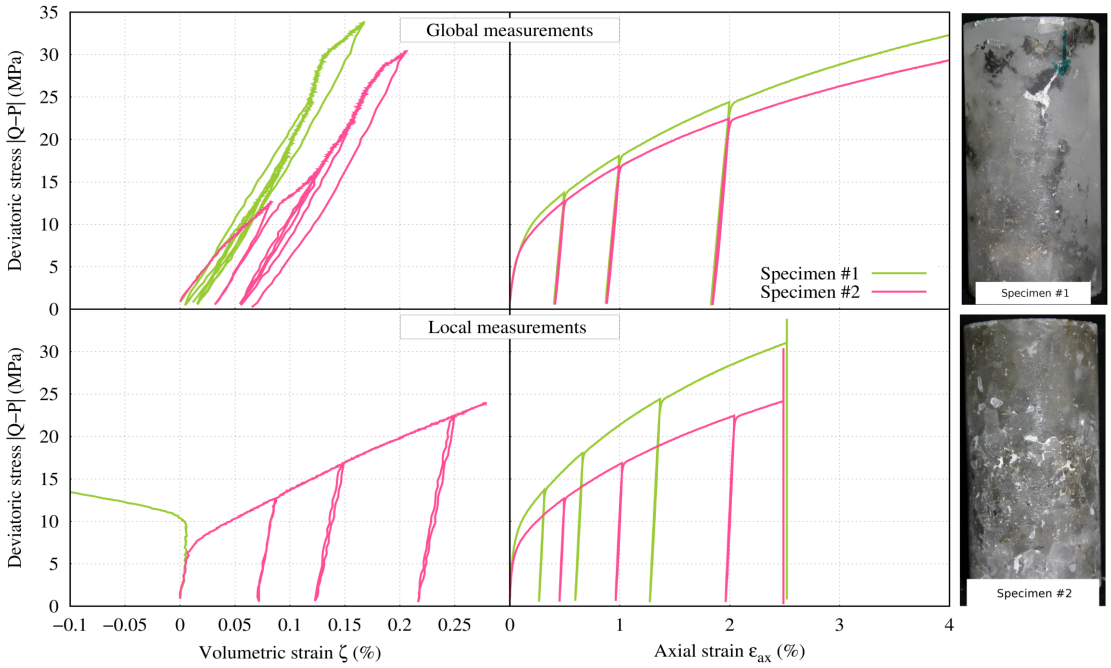

Figure 9: Results of two identical triaxial compression tests (P= 10 MPa, $\dot{\varepsilon}_{ax} = 2 \times 10^{-5}$ s^{-1}) and the corresponding tested salt specimens with difference in depths of 21.4 m.

2.2. *Discussion*

The analysis of these experimental data showed that it is possible for a specimen to display a local response that is significantly different from the global one. The malfunction of the measurement techniques is excluded: we have analyzed the results and confirmed that the gauges have been fully functional, we also assume that there were no oil leaks to alter the global measurement. Rouabhi et al. (2019) proved that the friction with the loading platens can in fact cause the local measurements to deviate from the global ones but not to the observed extent. This can be interpreted by the presence of material heterogeneity close to the placement of the gauges which capture very local phenomena due to their size.

We have also seen that specimens that are considered representative of a given rock salt, can show a very similar deviatoric behavior when subjected to the same loading conditions but a different volumetric behavior: the dispersion is always more pronounced in the local measurements. This implies that, especially in terms of the volumetric response, our specimens could be smaller than the required representative element volume (REV) for the studied rock salt.

Both of these observations can be traced back to the material spatial heterogeneity and among the many aspects of it (Chemin, 1990; Van-Hasselt, 1991; Thiemeyer et al., 2015; Speranza et al., 2016; Thiemeyer et al., 2016; Mansouri et al., 2019), we chose to focus this study on the presence of nodules of impurities similar to what can be seen on the specimen from Figure 4.
We investigate the effect of such heterogeneity on the volumetric behavior and the representativity of the used specimens. Rigorous experimental investigation of this aspect is problematic due to the following reasons:

- we do not have control over the material heterogeneity; as it was mentioned before, various aspects of heterogeneity exist within a salt sample which means that we cannot attribute a certain behavior to one particular aspect;

- the measured volumetric strains are extremely small (Roberts et al., 2015; Labaune, 2018; Rouabhi et al., 2019) which means the errors and uncertainties inherent to the laboratory work can be non negligible and can affect the measurements and therefore alter our interpretations and analysis;

- in order to further investigate the representativity of the specimens, we need to perform typical triaxial compression tests on bigger samples. This is often complicated due to the limitations of the experimental facilities: typically a lab is equipped with cells that can host specimens heaving at most 2 or 3 particular diameters (respecting the dimensions specified in Ulusay et al. (2007)), and it is unrealistic to have a new cell each time there is a need to characterize a different rock.

Consequently, we decided to use a virtual laboratory built on numerical modeling and simulation tools. This will allow to investigate the effect of this particular aspect of heterogeneity on rock salt dilatancy in an attempt to understand the mentioned observations.

3. Constitutive model

This model has been developed by Rouabhi et al. (2019). It assumes an additive decomposition of the total strain rate tensor $\underline{\underline{\dot{\varepsilon}}}_{vp}$ into tensile $\underline{\underline{\dot{\varepsilon}}}^{t}_{vp}$ and compressive $\underline{\underline{\dot{\varepsilon}}}^{c}_{vp}$ parts.
The compressive and tensile parts of the viscoplastic strain rate tensor $\underline{\underline{\dot{\varepsilon}}}_{vp}$ are decomposed in the basis $(\underline{\underline{I}}, \underline{\underline{J}}, \underline{\underline{K}})$ defined as

$$\underline{\underline{I}} = \underline{\underline{1}}/\sqrt{3}, \;\; \underline{\underline{J}} = \underline{\underline{\sigma}}'/\|\underline{\underline{\sigma}}'\|, \;\; \underline{\underline{K}} = (\sqrt{2}\underline{\underline{I}} + \ell\underline{\underline{J}} - \sqrt{6}\underline{\underline{J}}^2)/\sqrt{1-\ell^2} \tag{2}$$

where $\underline{\underline{\sigma}}'$ is the deviatoric part of the stress tensor $\underline{\underline{\sigma}}$; and $\ell = \sqrt{6}tr(\underline{\underline{J}}^3)$ is the third invariant of $\underline{\underline{\sigma}}'$.
Under compressive loading, the evolution law of $\underline{\underline{\dot{\varepsilon}}}^{c}_{vp}$ can be written as

$$\underline{\underline{\dot{\varepsilon}}}^{c}_{vp} = -\sqrt{1/3}\dot{\zeta}^{c}_{vp}\underline{\underline{I}} + \sqrt{3/2}\dot{\gamma}^{c}_{vp}\underline{\underline{N}}^{c} \tag{3}$$

where $\dot{\zeta}^{c}_{vp} = -tr(\underline{\underline{\dot{\varepsilon}}}^{c}_{vp})$ and $\dot{\gamma}^{c}_{vp} = \sqrt{2/3}\|\underline{\underline{\varepsilon}}^{c}_{vp}{}'\|$ are the rates of the volumetric strain and the viscoplastic distorsion, respectively and $\underline{\underline{N}}^{c}$ is a unit tensor defining the deviatoric flow direction under compressive loading.
Under tensile loading, the strain rate tensor $\underline{\underline{\dot{\varepsilon}}}^{t}_{vp}$ is assumed to be described by a mechanism of Rankine-type:

$$\underline{\underline{\dot{\varepsilon}}}^{t}_{vp} = \dot{\lambda}\frac{\partial G}{\partial \underline{\underline{\sigma}}} \tag{4}$$

with

$$G = (\langle\sigma_1\rangle^d + \langle\sigma_2\rangle^d + \langle\sigma_3\rangle^d)^{1/d} \tag{5}$$

where $\dot{\lambda}$ is a positive multiplier, $\langle . \rangle$ are the Macaulay brackets, i.e. $\langle x\rangle = (x+|x|)/2$; $\sigma_1 \geq \sigma_2 \geq \sigma_3$ are the principal stresses of $\underline{\underline{\sigma}}$; and $d \geq 1$ is a constant parameter.
When the gradient of G with respect to $\underline{\underline{\sigma}}$ is written in the basis $(\underline{\underline{I}}, \underline{\underline{J}}, \underline{\underline{K}})$, Equation 4 can be rewritten as:

$$\underline{\underline{\dot{\varepsilon}}}^{t}_{vp} = -\sqrt{1/3}\dot{\zeta}^{t}_{vp}\underline{\underline{I}} + \sqrt{3/2}\dot{\gamma}^{t}_{vp}\underline{\underline{N}}^{t} \tag{6}$$

with

$$\dot{\zeta}^{t}_{vp} = -\dot{\lambda}X, \;\; \dot{\gamma}^{t}_{vp} = \dot{\lambda}\sqrt{Y^2+Z^2} \tag{7}$$

where $\underline{\underline{N}}^{t}$ defines the deviatoric flow direction under tensile loading and the quantities X, Y and Z are such that

$$\begin{cases} X = G_1' + G_2' + G_3' \\ Y = (2G_1' - G_2' - G_3')/3 \\ Z = (G_2' - G_3')/\sqrt{3} \end{cases} \tag{8}$$

with $G_i' = \langle \sigma_i / G \rangle^{d-1}$ the eigenvalues of $\partial G / \partial \underline{\underline{\sigma}}$.

Finally, the additive decomposition of the total strain rate tensor $\dot{\underline{\underline{\varepsilon}}}_{vp}$ into tensile $\dot{\underline{\underline{\varepsilon}}}^t_{vp}$ and compressive $\dot{\underline{\underline{\varepsilon}}}^c_{vp}$ parts, leads to

$$\dot{\underline{\underline{\varepsilon}}}_{vp} = -\sqrt{1/3}\dot{\zeta}_{vp}\underline{\underline{I}} + \sqrt{3/2}\left(\dot{\gamma}^c_{vp}\underline{\underline{N}}^c + \dot{\gamma}^t_{vp}\underline{\underline{N}}^t\right) \tag{9}$$

with $\dot{\zeta}_{vp} = \dot{\zeta}^c_{vp} + \dot{\zeta}^t_{vp}$. As can be seen from this Equation, the tensile contribution acts on both components of $\dot{\underline{\underline{\varepsilon}}}_{vp}$, volumetric and deviatoric.

To fully define $\dot{\underline{\underline{\varepsilon}}}_{vp}$, $\dot{\gamma}^c_{vp}$, $\dot{\zeta}^c_{vp}$ and $\dot{\lambda}$ need to be defined, which will be done as follows.

For the compressive part, the evolution law of $\dot{\zeta}^c_{vp}$ is expressed as

$$\dot{\zeta}^c_{vp} = \psi\left(\underline{\underline{\sigma}}, \gamma^c_{vp}\right)\dot{\gamma}^c_{vp} \tag{10}$$

with

$$\psi\left(\underline{\underline{\sigma}}, \gamma^c_{vp}\right) = z\frac{\left\langle p/N \right\rangle^n - \gamma^c_{vp}}{\left\langle p/M \right\rangle^m + \gamma^c_{vp}} \tag{11}$$

and γ^c_{vp} is given through a generalization of Lemaitre model (Tijani et al., 1983), enriched with an influence of the mean pressure p and the Lode angle θ:

$$\frac{d\left(\gamma^c_{vp}\right)^{1/a}}{dt} = \left\langle \left[q/\varrho(\theta) - \left(\gamma^c_{vp}\right)^b Bp - C \right] \Big/ K \right\rangle^{k/a} \tag{12}$$

In Equation 11, the sign of $\langle p/N \rangle^n - \gamma^c_{vp}$ indicates whether the behavior is contracting or dilating.

Regarding the tensile part, we consider an evolution law of Perzyna-type:

$$\dot{\lambda} = \Lambda \langle (G - R_t)/S \rangle^s \tag{13}$$

In Equations 11 to 13, $z, n, m, a, b, B, C, K, k, \Lambda, R_t, d, s, M, N$ and S are the material parameters.

When this model is used to simulate a triaxial compression test, dilatancy is:

- taken into account on a constitutive level when we assume that the stress field within the specimen is homogeneous and all stresses are compressive (Equations 10 and 11);
- a result of a heterogeneous distribution of the stress field leading to activating the tension mechanism (Equations 7 and 13).

4. Numerical Investigations

We first present and validate our numerical approach which is then employed to investigate the volumetric strains measured by different measurement techniques on a salt specimen containing nodules of impurities. The natural variability, its effect on the volumetric strain measurements and the specimens representativity are discussed in section 4.3.

4.1. Structural approach for dilatancy

The micro structure of a salt specimen in reality is very complex to be reproduced numerically (different grain sizes, fluid inclusions, grain boundaries, different types and shapes of heterogeneities,...). In this work, we assume that salt is a two-phase medium composed of a pure halite matrix and nodules of insoluble materials. This simplifying assumption is accepted, since the aim of this research is to qualitatively understand the impact of the presence of heterogeneities on the macroscopic behavior. Thus the numerical validation of the approach does not concern its ability to reproduce the complex geometry of real salt specimens, but rather the measurements of physical quantities.

A salt specimen is modeled as a cylindrical matrix of pure halite, with inclusions representing the nodules of insolubles as shown in Figure 10. The insolubles are modeled as spheres for the sake of simplicity and the specimens are generated as follows. First, a cube's side length, the volume fraction of insolubles within the cube, the minimum and maximum radii (of the inclusions) are designated. Second, an iterative process allows to generate, via a uniform random number generator, the position of a sphere center (within the cube) and a radius (between the specified bounds); the respect of the specified volume fraction is checked at each iteration. Finally, once the distribution of the spheres is generated within the cube, the position and size of the specimen to model are chosen and the virtual sampling is performed.

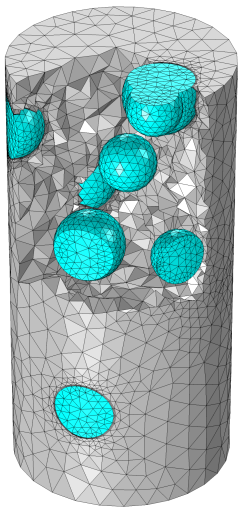

Figure 10: Cutaway view of the modeled structure of a salt specimen with nodules of insolubles.

The structure shown in Figure 10 will be used as a reference specimen for our numerical investigations. It contains a volume fraction of inclusions of $\phi = 10.3\%$, the density of the halite matrix is assumed to be 2160 kg/m^3 which leads to a mass fraction of $w = 8.3\%$. Such mass fraction is within the usual ranges found in salt rocks (Gillhaus et al., 2006). The insolubles are considered to have properties similar to clay: a density of $\rho = 1700$ kg/m^3, a Young's modulus of $E = 5000$ MPa and a Poisson's ratio of $\nu = 0.32$.

We assume the continuity of the displacement field within the structure, and we do not introduce a joint model for the interface halite-inclusions. This simplifying assumption was made because on one hand the joint parameters are difficult to determine experimentally and on the other hand, introducing additional parameters will further complicate the study especially with the meshing requirement of the modeled structures. The assumption is valid since, as will be shown through this paper, the macroscopic aspects of rock salt behavior are reproduced.

The behavior of the insolubles is assumed to be linear elastic while the salt matrix is governed by the constitutive law presented in section 3.The parameter set used for the salt matrix is presented in Table 1. This parameter set was adopted from Labaune (2018) where the distorsion and dilatancy parameters were obtained by fitting triaxial compression and creep tests, and fitting a Brazilian test provided the ones relative to the tension mechanism. In this work, some of these parameters

are changed. The tensile strength is set to $R_t = 0$ (Equation 13) in compliance with setting the cohesion $C = 0$ (Equation 12). Also, setting the parameter $B = 0$ (Equation 12) means that we omit the mean pressure effect and setting $z = 0$ (Equation 11) implies that the viscoplastic volumetric strain due to compressive stresses is not considered. The tensile part is deactivated by setting the parameter $\Lambda = 0$ (Equation 13).

Elasticity					
E	ν				
20000	0.32				
Distorsion					
a	k	b	B	K	C
0.29	2.2	0.24	0	0.13	0
Dilatancy					
z	n	N	m	M	
0	1.3	0.012	3.3	1.37	
Tension					
d	Λ	R_t	S	s	
10	0	0	1	1	

Table 1: Parameters used to simulate the behavior of the salt matrix. The unit system is such that strain is in μm/m, stress is in MPa and time in days.

We used VIPLEF3D, a finite element code developped in the Geosciences Department of Mines ParisTech(Tijani, 2008) to simulate a typical triaxial test on the structure shown in Figure 10. The simulated test is conducted under a constant strain rate of 10^{-6} s^{-1} and a confining pressure of 5 MPa.

The results showed that within the salt matrix and around the spherical inclusions, zones where the principal major stress σ_1 is positive appear and continue to develop all along the simulation. Figure 11 shows the distribution of σ_1 within the salt matrix at an axial strain $\varepsilon_{ax} \approx 2\%$: the difference in rigidity of the inclusions and the halite matrix led to the appearance of tensile zones and to stress concentrations.

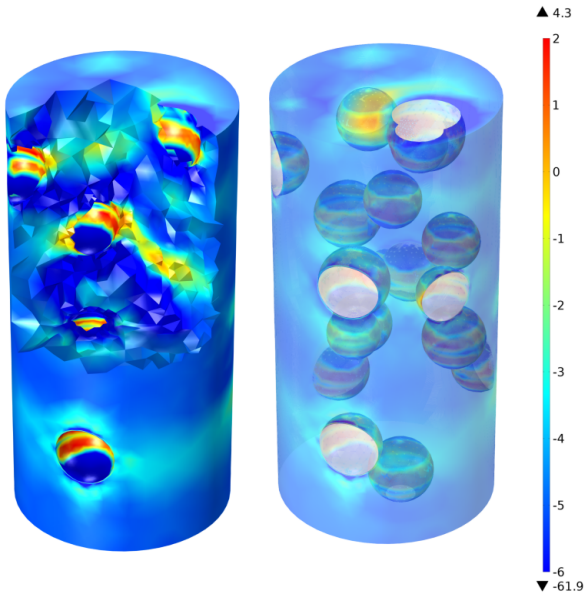

Figure 11: Cutaway (left) and transparent (right) views of the distribution of σ_1 (MPa) within the salt matrix at $\varepsilon_{ax} \approx 2\%$ (simulation of a typical triaxial compression test under a confinement of 5 MPa and an axial strain rate of 10^{-6} s^{-1}, on the specimen shown in Figure 10).

Because of these results, we re-conducted the same simulation except for activating the tensile part this time (the parameter Λ from Equation 13 was set to 5×10^4). Activating this component of the viscoplastic strain tensor means that in the halite matrix, irreversible strains are of two kinds: those governed by the deviatoric creep mechanism and those governed by the tensile mechanism, which obviously vanish under compressive loadings when the assumption of stress homogeneity usually made in the analysis of laboratory tests, is used.

The obtained results of the two performed simulations in terms of global measurements are given in Figure 12.

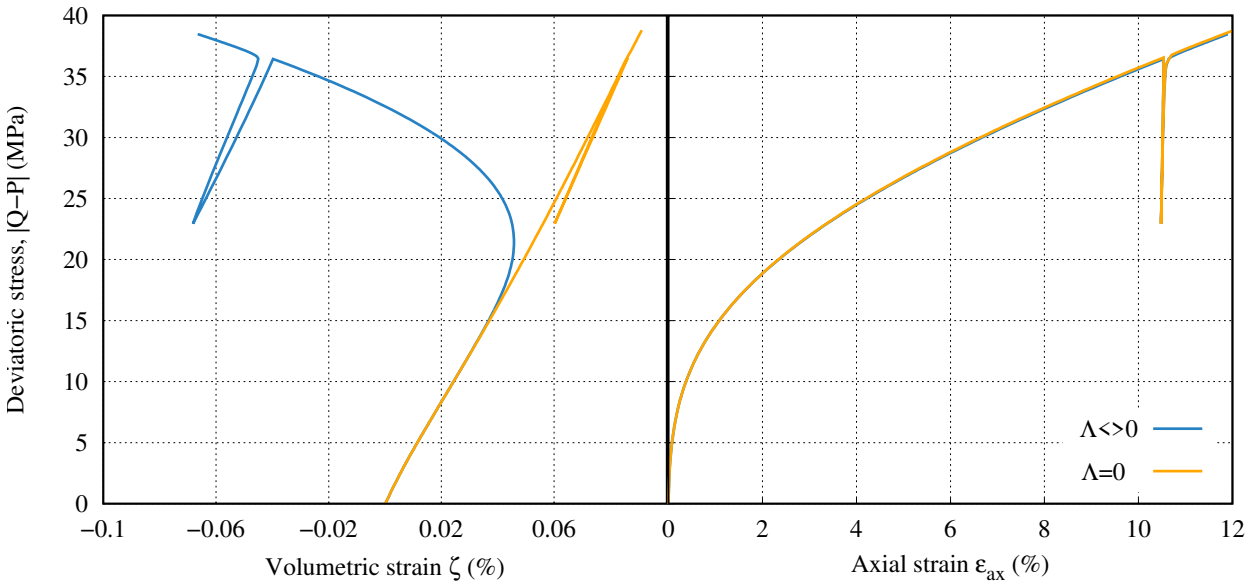

Figure 12: Results of simulations of a typical triaxial compression test under a confinement of 5 MPa and an axial strain rate of 10^{-6} s^{-1}, on the specimen shown in Figure 10.

The overall behavior of the structure has the same characteristics observed in the lab for salt specimens during this type of tests: viscoplastic hardening, contractancy and dilatancy. This is an important result because it shows that dilatancy can be a consequence of the material spatial heterogeneity. In fact in this study, the presence of heterogeneities lead to the development of stress concentrations and induced tensile stress zones which physically reflect the occurrence of a micro-cracking activity and therefore dilatancy. We still need to validate the ability of the approach to reproduce other characteristics like the mean pressure and the loading rate effects and most importantly the creep behavior. We use the reference specimen from Figure 10 to simulate a series of lab tests, as listed in Table 2.

Studied Aspect	$\dot{\varepsilon}_{ax}$ [s^{-1}]	P [MPa]	Stages of $\lvert Q-P\rvert$ [MPa]
Effect of loading rate	10^{-6}, 5×10^{-6}, 10^{-5}	5	-
Effect of the mean pressure	10^{-6}	0, 5, 10, 15	-
Creep behavior	-	5	5, 10

Table 2: Lab tests simulated on the specimen shown in Figure 10.

The results of these simulations are shown in Figures 14 to 15 and are considered very satisfactory as both effects of loading rate and mean pressure are correctly predicted. In fact, the dilatancy limit increases with the mean pressure (equivalent to confining pressure effect) and is significantly affected by the loading rate: the slower the test the lower the dilatancy limit (Labaune et al., 2018). Also the creep behavior is very similar to what is typically seen in the lab (Günther et al., 2015; Labaune et al., 2018).

These results have been obtained as well for other structures with different inclusions shape, distribution, size, volume fraction and different elastic constants. This approach is then assumed to be valid to describe rock salt behavior in the lab.

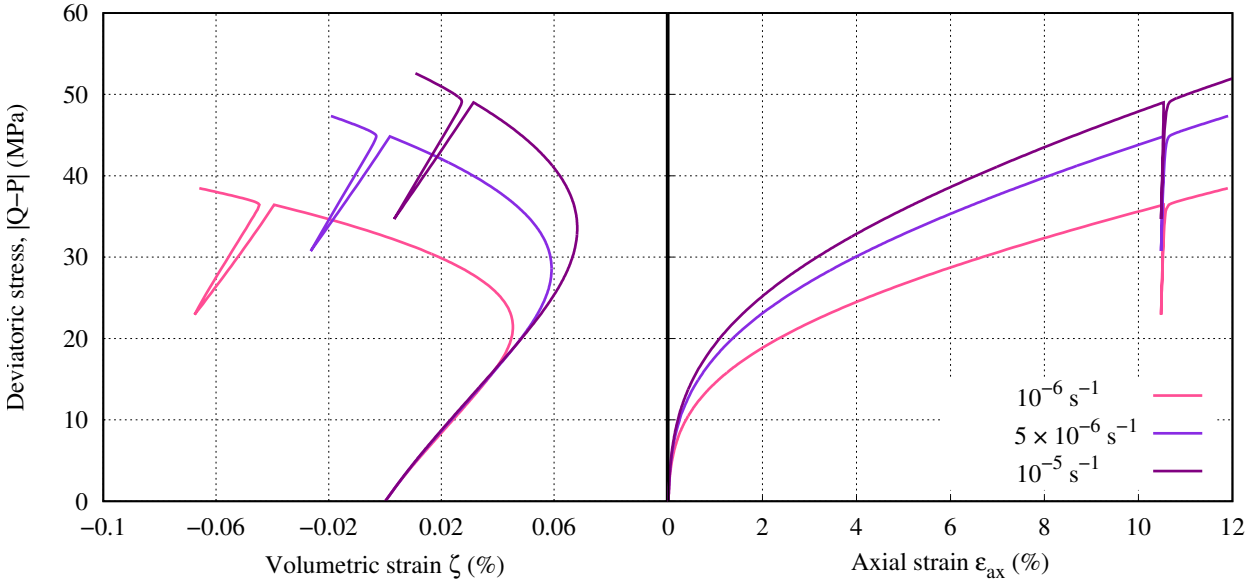

Figure 13: Results of simulations of typical triaxial tests (P=5 MPa) on the specimen in Figure 10 : effect of loading rate.

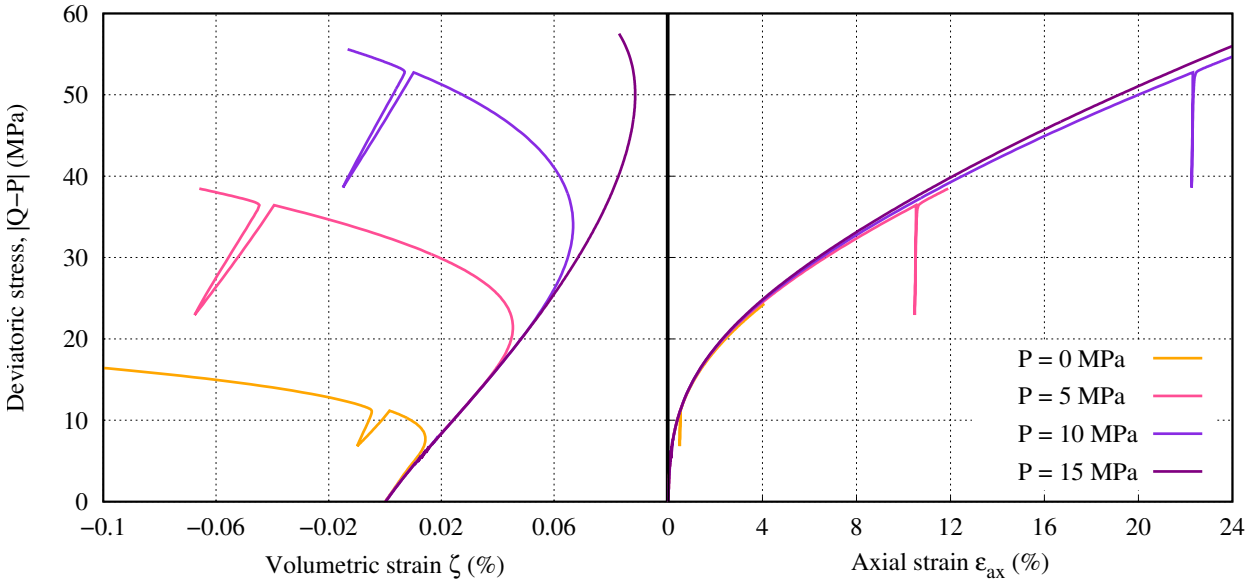

Figure 14: Results of simulations of typical triaxial tests ($\dot{\varepsilon}_{ax} = 10^{-6}$ s^{-1}) on the specimen in Figure 10 : effect of confining pressure.

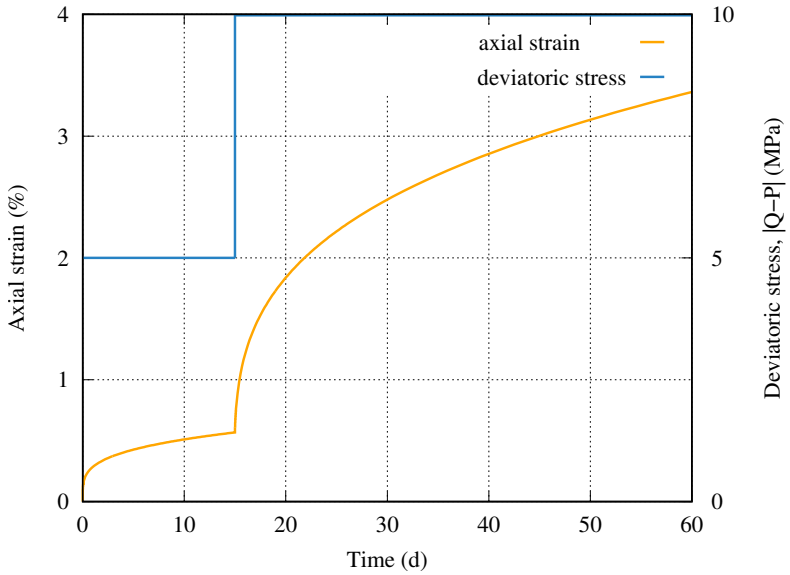

Figure 15: Results of a simulation of a typical triaxial multistage creep test (P=5 MPa) on the specimen in Figure 10.

4.2. Volumetric strain measurements on a heterogeneous specimen

We adopt the approach detailed in section 4.1 and the same parameter set given in Table 1 for the numerical study hereafter where we try to understand the experimental observations and obtain a qualitative assessment of the effect of heterogeneities on the volumetric behavior of rock salt. We simulated on the reference specimen in Figure 10, a conventional triaxial test under a confining pressure of 5 MPa and a constant axial strain rate of $10^{-6}s^{-1}$ (see Figure 13). We modeled the placement of two sets of strain gauges on the specimen in an attempt to get local strain measurements with the same procedure used in the lab. We have randomly chosen the position of the two sets of gauges, the only conditions were that the sets have to be placed at mid-height and on the salt matrix's lateral surface. We chose to investigate the effect of the friction with the platens as well so the simulation was conducted twice with the two extreme conditions of specimen-platen contact: smooth contact with no friction between the specimen and the loading platens and rough contact where there is a complete radial restraint on the specimen ends. This last boundary condition causes the initially right cylinder specimen to deform into a barrel (triaxial compression) or an hourglass (triaxial extension) shape (Labaune, 2018; Rouabhi et al., 2019). Figure 16 shows the obtained results.

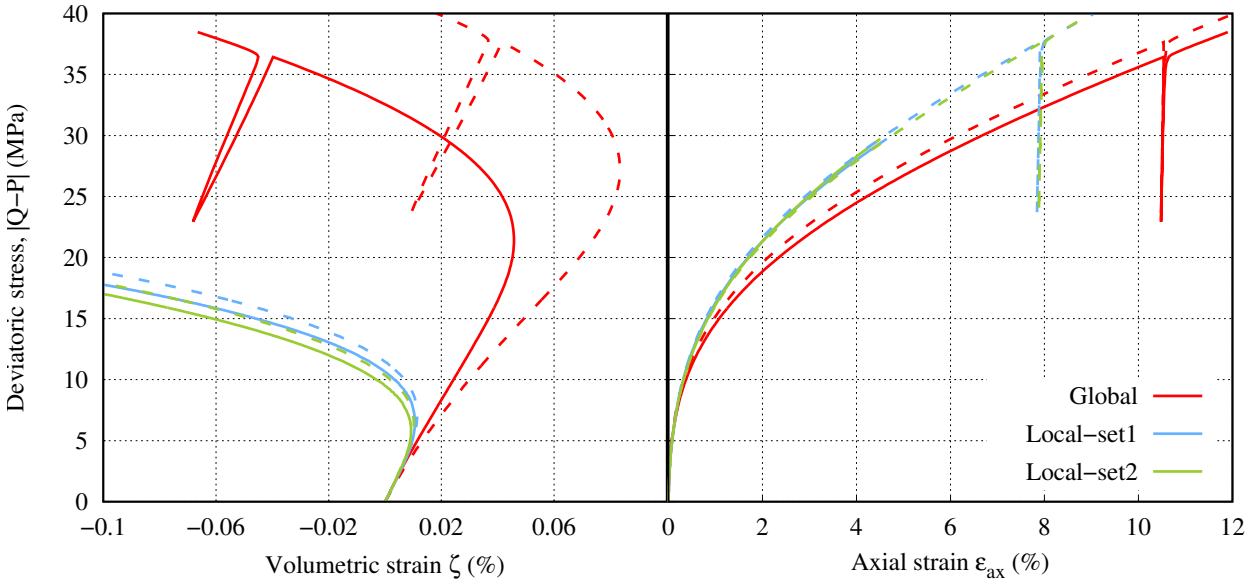

Figure 16: Results of a simulation of a typical triaxial compression test (P=5 MPa and $\dot{\varepsilon} = 10^{-6}$ s^{-1}) on the specimen in Figure 10. Curves in dashed and continuous lines correspond respectively to simulations with and without accounting for the friction with the loading platens.

These results show that the friction with the platens significantly affects the global volumetric strain measurements but it has a slight impact on the axial and the local volumetric strain measurements. The sets of gauges give very similar results in terms of both axial and volumetric strains, in fact this specimen does not have locations of inclusions concentration, instead the spheres are almost evenly distributed (see the transparent view in Figure 10). This leads to a sort of uniformity over the lateral surface : all gauges placed at mid-height of the specimen are likely to give very similar measurements; no gauge could be significantly more exposed to inclusions than others.
We often have specimens were the inclusions are not evenly distributed as can be seen on the specimen in Figure 4: in this sample we can see that there are areas on the lateral surface that are covered with insolubles and others that are almost clear. To study such cases, we conduct the same simulation on the specimen presented in Figure 17. In this case, we placed the first set of gauges near the inclusion we see on the lateral surface of the specimen and the second set on the opposite side (relatively furthest from inclusions). The results are shown in Figure 17.

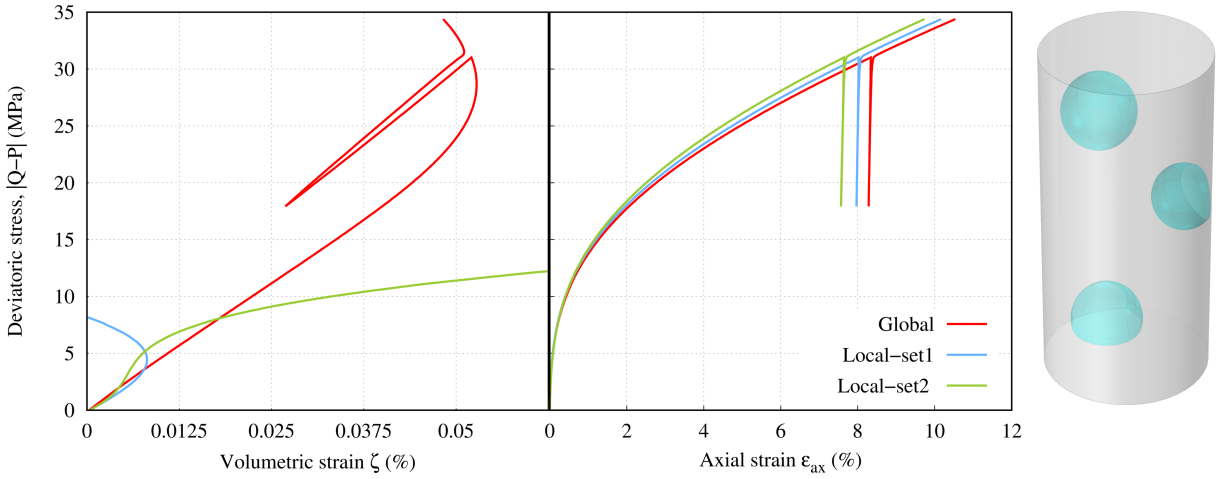

Figure 17: Results of a simulation of a typical triaxial compression test (P=5 MPa and $\dot{\varepsilon} = 10^{-6}$ s^{-1}) and the corresponding specimen.

We see similarly to what has been noted at the lab, the axial strain measurement is slightly affected, the dispersion shown between global and local measurements is acceptable. Regarding the volumetric strains, the difference is out of the usual ranges and patterns (see Figure 2). At a deviatoric stress level of ≈ 4 MPa, the first set (closest to the inclusions) measures significantly important radial strains due to the local appearance of tensile stresses (see Figure 11) and we see a local dilatancy onset. On the other hand, the second set (furthest from the inclusions) only sees contractancy until the end of the simulation: the radial strains in that location of the specimen were never important because tensile stresses did not appear there. It is not until the deviatoric stress reaches ≈ 27 MPa that the whole specimen's volume begins to increase. The information provided by the sets of gauges are true but have unexpected patterns and dilatancy onset values because they capture very local phenomena.

In this investigation we have provided a possible interpretation to cases like the ones presented in Figures 3 and 6. We have also given a possible explanation to one of the main conclusions of Rouabhi et al. (2019) which states that the friction with the loading platens cannot explain the difference observed between local and global measurements of the volumetric strain.

4.3. Natural Variability and Specimens Representativity

In this section, we investigate the representativity of specimens from a volumetric point of view. We generate a random distribution of spheres with radii ranging from 8 to 20 mm within $\approx 7\%$ of the volume of a 20 cm side length cube. As shown in Figure 18, we virtually sample this cube and generate 4 salt specimens that are 13 cm high with a diameter of 6.5 cm. The inclusions and the halite matrix have the properties mentioned in section 4.1. The mass fraction of insolubles in each specimen is indicated in Figure 18 as well.

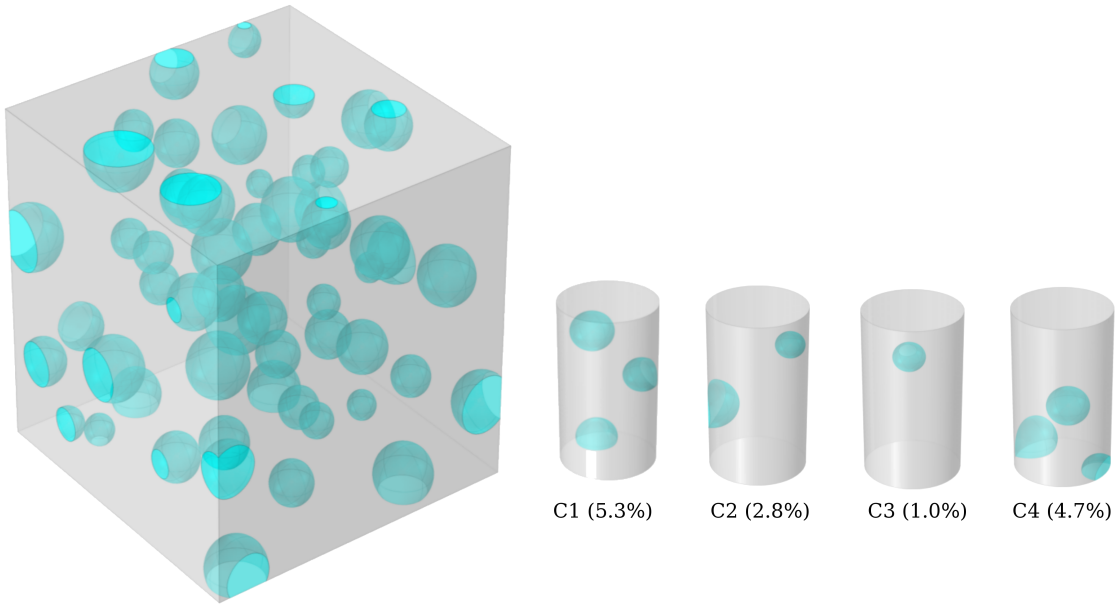

Figure 18: A modeled salt block with virtually sampled specimens, the mass fraction of insolubles is indicated for each specimen.

For each of the four shown specimens, we simulate a conventional triaxial compression test where the axial strain rate is fixed at $10^{-6}s^{-1}$ and the confining pressure at 5 MPa. The simulations continued until dilatancy onsets were globally seen. The results are shown in Figure 19 in terms of global measurements.

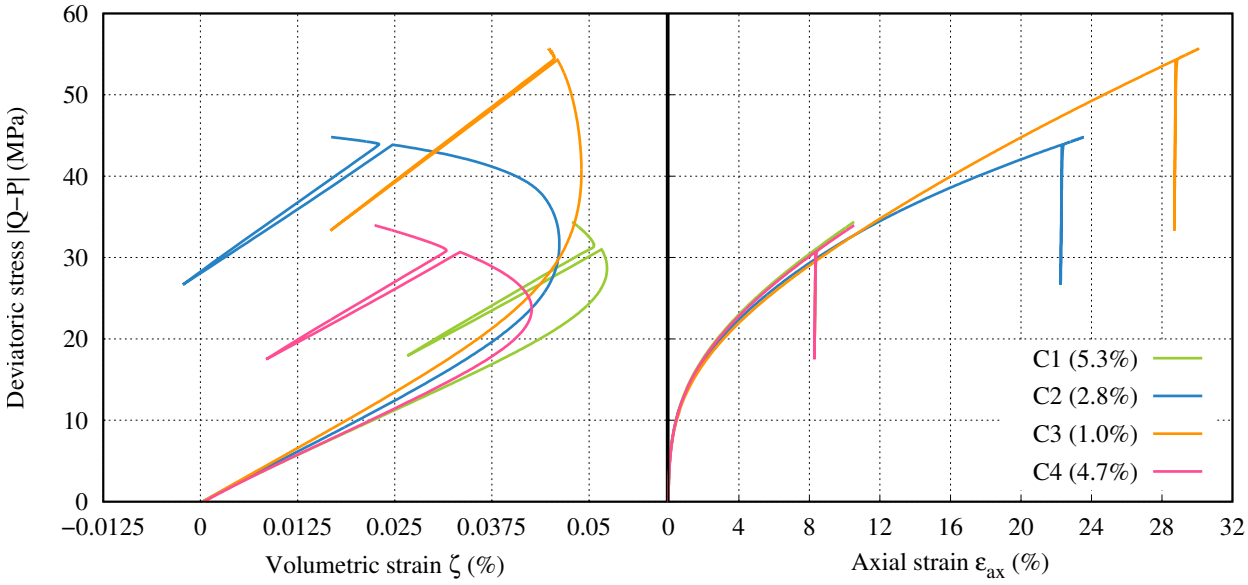

Figure 19: Results of a conventional triaxial compression test (P=5 MPa and $\dot{\varepsilon} = 10^{-6}$ s^{-1}), on the specimens shown in Figure 18.

As shown in Figure 19, the axial strain measurements present slight deviations, while the volumetric ones are significantly different. Because of the size of the insolubles and their distribution within the initial block, none of the sampled specimens were representative of the block from a volumetric perspective. Testing bigger specimens might seem like an immediate and ideal solution for this issue. However in practice, we may be constrained by the geometry of the available triaxial cells as explained in section 2 and we may even face cases where the maximum testable size (diameter equal to the coring diameter and a slenderness ratio of two) is not representative of the rock in question. Besides, testing bigger specimens is likely to compromise the precision of the obtained strain measurements; in fact the bigger the specimen, the bigger the required volume of confining oil and the less accurate the obtained volumetric strain measurements.

We study a second case scenario, where we generate a random distribution of spheres with radii ranging from 5 to 10 mm within $\approx 5\%$ of the volume of a 20 cm side length cube. As shown in Figure 20, we virtually sample this cube and generate 3 salt specimens that are 13 cm high with a diameter of 6.5 cm. Using the same properties for the inclusions and the halite matrix as the previous case, the mass fraction of insolubles in each specimen is indicated in Figure 20. We simulate

the same test as performed on the specimens shown in Figure 19 and we present the corresponding results in Figure 21.

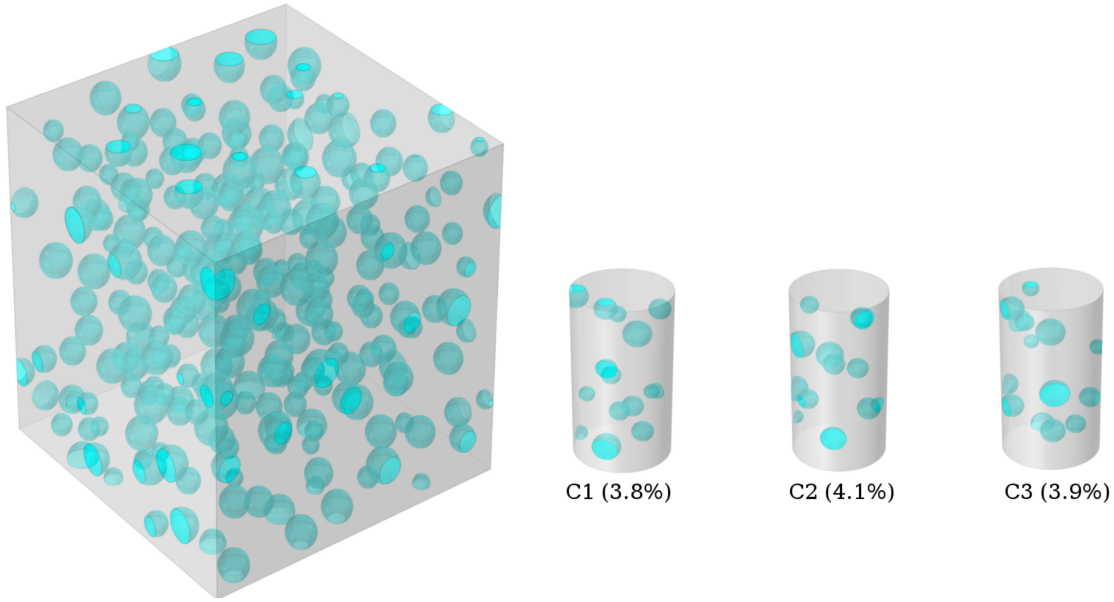

Figure 20: A modeled salt block with virtually sampled specimens, the mass fraction of insolubles is indicated for each specimen

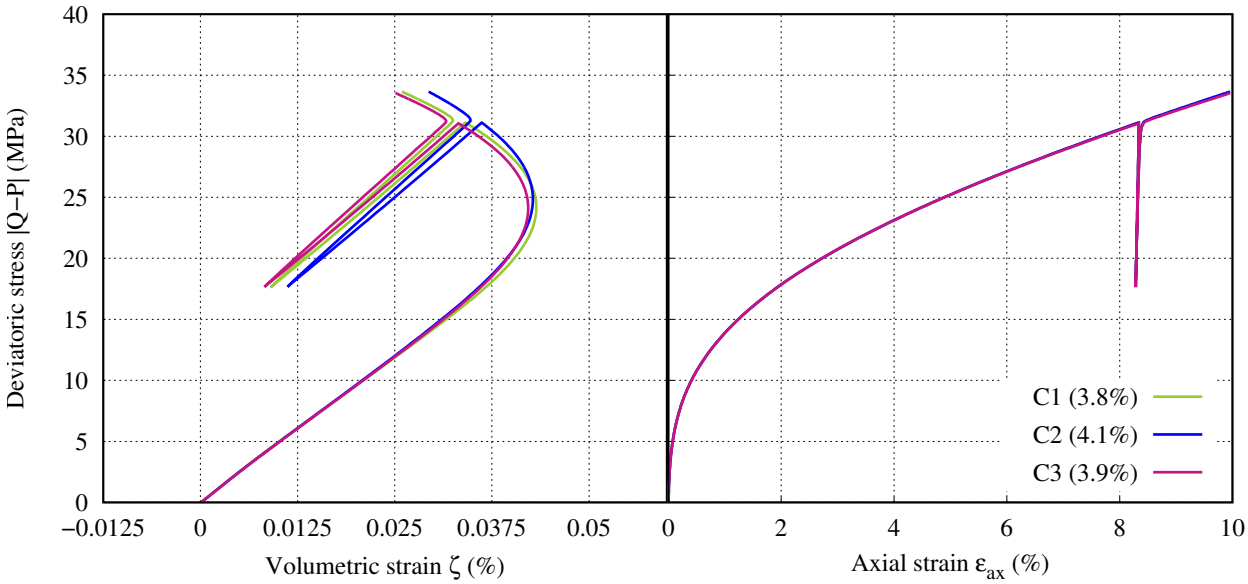

Figure 21: Results of a conventional triaxial compression test (P=5 MPa and $\dot{\varepsilon} = 10^{-6}$ s^{-1}), on the specimens shown in Figure 20.

In this case, the inclusions size is small compared to the dimensions of the specimen, in fact for all three of the cases we have $R_{max}/R_{spec} \approx 0.29$ where R_{max} is the radius of the largest sphere included within the halite matrix and R_{spec} is the radius of the specimen. Besides there are more inclusions in these specimens (14 for C1, 12 for C2 and 13 for C3) than the ones from the first scenario (Figure 18) and they are evenly distributed within the volumes. These reasons lead to the fact that we see almost no dispersion neither in the axial nor in the volumetric strain measurements : we are addressing an equivalent homogeneous material. Consequently in similar cases, we can safely adjust a phenomenological model and use the resulting parameter set for the concerned underground facility.

To illustrate this, we use the same constitutive model introduced in section 3 to fit the curve C1 in Figure 21. We assume that the stress and strain fields within the specimen are homogeneous, all the stresses are compressive and therefore the tensile mechanism cannot be activated. We set $z \neq 0$ in order to reproduce the volumetric strain. In other words, the results shown in Figure 21 for the specimen C1, are considered experimental data to fit with the the proposed model under the assumptions stated. Figure 22 shows the fitting of these data with the parameter set given in Table 3. As it can be seen, the phenomenological model, where dilatancy is taken into account on a constitutive level, matches very well the results.

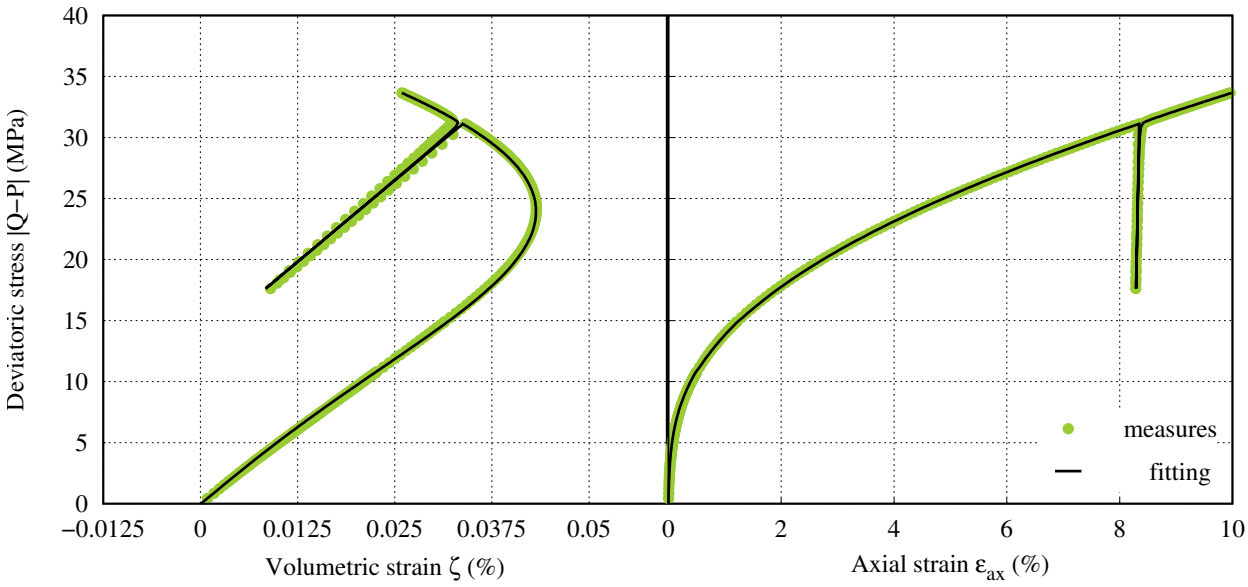

Figure 22: Fitting of a conventional triaxial compression test (P=5 MPa and $\dot{\varepsilon} = 10^{-6}$ s^{-1}) conducted on specimen C1 shown in Figure 20.

Elasticity					
E	ν				
22523	0.29				
Distorsion					
a	k	b	B	K	C
0.21	2.7	0.29	0.03	0.1	0
Dilatancy					
z	n	N	m	M	
1.3	1.07	0.0012	2.05	0.0058	
Tension					
d	Λ	R_t	S	s	
10	0	0	1	1	

Table 3: Parameters used to fit the triaxial test results C1 shown in Figure 21. The unit system is such that strain is in μm/m, stress is in MPa and time in days.

5. Conclusions

In this paper, the volumetric strain measurements were experimentally investigated through the analysis of over 120 typical triaxial compression tests on salt specimens from different locations. The difference between local and global measurements exhibited during this analysis, raised questions concerning the effect of material spatial heterogeneity on the volumetric behavior and consequently on the representativity of the used specimen. We chose to focus on a specific aspect of material heterogeneity: the presence of nodules of insoluble materials within a pure halite matrix, in order to obtain a qualitative understanding of the issue.

We carried out a numerical study during which salt specimens were considered as cylindrical matrices of pure halite with spherical inclusions. We proved that dilatancy can be a consequence of the specimen's material heterogeneity.

We then investigated the experimental observations and proved that the significant differences (in patterns and the measured dilatancy onsets) between local and global volumetric strain measurements, were satisfactorily explained by the material spatial heterogeneity.

Finally, we ~~have shown~~ found that the presence of nodules of insoluble materials within a salt rock could lead to representativity issues. And in that case, we propose the following general methodology :

1. Characterize one of the used specimens (known to be not representative): volume fraction of insoluble materials, the nature of the inclusions (thus getting an estimation of their elastic constants), the concentration zones of heterogeneity.

2. Model this specimen as ~~a structure as described in the beginning of section 4.1: a pure halite matrix with nodules of impurities.~~a two-phase medium composed of a pure halite matrix and nodules of insolubles.

3. Perform a history matching of the experimental data with a given constitutive model (in which dilatancy results from the activation of a tensile mechanism induced by the presence of heterogeneities) on the modeled structure.

4. Once a parameter set is obtained, ~~we~~ model a representative specimen: containing much more inclusions of a negligible size compared to the dimensions of the specimen ~~(similar to what is shown in Figure 20)~~.

5. Simulate the test conducted in the lab on the representative specimen using the same constitutive model from step 3 ~~the approach described in section 4.1~~ with the parameter set resulting from the ~~previous~~ history matching.

6. The obtained results are supposed to be representative of the rock in question. They can be fit with a given phenomenological constitutive model ~~with the considerations taken in the fittings of section 4.3~~assuming the homogeneity of the stress field. Dilatancy in the chosen model should be taken into account on a constitutive level.~~: t~~ The resulting parameter set can then be used for the corresponding rock salt.

This methodology combines experimental work with numerical modeling in order to overcome specimens representativity issues and the limitations of laboratory testing procedures.

Acknowledgments

The authors would like to thank their colleagues Michel Tijani and Faouzi Hadj-Hassen from MINES ParisTech for their valuable contributions.

References

Bays, C. A., 1963. Use of salt cavities for underground storage. In: Symposium on Salt.; Northern Ohio Geological Society. Cleveland, Ohio, pp. 564–578.

Chemin, P., Nov. 1990. Etude du rôle des inclusions fluides dans les mécanismes de déformation des roches halitiques. Application aux formations salifères du bassin bressan. Theses, Ecole Nationale des Ponts et Chaussées.

DeVries, K., Mellegard, K., October 2010. Effect of specimen preconditioning on salt dilation onset. In: SMRI fall 2010 technical conference. Leipzig, Germany.

DeVries, K., Mellegard, K., Callahan, G., Goodman, W., 2005. Cavern roof stability for natural gas storage in bedded salt. Technical report de-fg26-02nt41651, RESPEC, Rapid City, South Dakota.

DeVries, K. L., Mellegard, K. D., Callahan, G. D., 11 2002. Salt damage criterion proof-of-concept research. Technical report rsi-1675 de-fc26-00nt41026, RESPEC, Rapid city, South Dakota.

Gillhaus, A., Crotogino, F., Albes, D., 2006. Compilation and evaluation of bedded salt cavern characteristics important to successful cavern sealing, part 1: Worldwide bedded slat deposits and bedded salt cavern characteristics. 2003-5-smri.solution mining research institute research project report.

Günther, R.-M., Salzer, K., Popp, T., Lüdeling, C., 09 2015. Steady-state creep of rock salt: Improved approaches for lab determination and modelling. Rock Mechanics and Rock Engineering 48.

Habibi, R., 2019. An investigation into design concepts, design methods and stability criteria of salt caverns. Oil Gas Sci. Technol. - Rev. IFP Energies nouvelles 74, 14.

Heusermann, S., Rolfs, O., Schmidt, U., 2003. Nonlinear finite-element analysis of solution mined storage caverns in rock salt using the lubby2 constitutive model. Computers Structures 81 (8), 629 – 638, k.J Bathe 60th Anniversary Issue.

Hou, Z., 2003. Mechanical and hydraulic behavior of rock salt in the excavation disturbed zone around underground facilities. International Journal of Rock Mechanics and Mining Sciences 40 (5), 725 – 738.

Labaune, P., 10 2018. Comportement thermomécanique du sel gemme : Application au dimensionnement des cavités. Ph.D. thesis.

Labaune, P., Rouabhi, A., Tijani, M., Blanco-Martín, L., You, T., Feb 2018. Dilatancy criteria for salt cavern design: A comparison between stress- and strain-based approaches. Rock Mechanics and Rock Engineering 51 (2), 599–611.

Mansouri, H., Prior, D. J., Ajalloeian, R., Elyaszadeh, R., 2019. Deformation and recrystallization mechanisms inferred from microstructures of naturally deformed rock salt from the diapiric stem and surface glaciers of a salt diapir in southern iran. Journal of Structural Geology 121, 10 – 24.

Medina-Cetina, Z., Rechenmacher, A., 01 2009. Influence of boundary conditions, specimen geometry and material heterogeneity on model calibration from triaxial tests. International Journal for Numerical and Analytical Methods in Geomechanics 34, 627–643.

Mellegard, K., Callahan, G., Devries, K. L., 01 2005. Lode angle effects on the deformational properties of natural

rock salt. In: American Rock Mechanics Association.

Munson, D., Dawson, P., 1981. Salt constitutive modeling using mechanism maps. In: First conference on the mechanical behavior of salt. pp. 717–737.

Popp, T., Kern, H., 1998. Ultrasonic wave velocities, gas permeability and porosity in natural and granular rock salt. Physics and Chemistry of the Earth 23 (3), 373 – 378.

Roberts, L. A., Buchholz, S. A., Mellegard, K. D., Düsterloh, U., Nov 2015. Cyclic loading effects on the creep and dilation of salt rock. Rock Mechanics and Rock Engineering 48 (6), 2581–2590.

Rouabhi, A., Labaune, P., Tijani, M., Gatelier, N., Hévin, G., 2019. Phenomenological behavior of rock salt: On the influence of laboratory conditions on the dilatancy onset. Journal of Rock Mechanics and Geotechnical Engineering.

Schulze, O., Popp, T., Kern, H., 2001. Development of damage and permeability in deforming rock salt. Engineering Geology 61 (2), 163 – 180, geosciences and Nuclear Waste Disposal.

Speranza, G., Vona, A., Vinciguerra, S., Romano, C., 2016. Relating natural heterogeneities and rheological properties of rocksalt: New insights from microstructural observations and petrophyisical parameters on messinian halites from the italian peninsula. Tectonophysics 666, 103 – 120.

Stormont, J., 1997. In situ gas permeability measurements to delineate damage in rock salt. International Journal of Rock Mechanics and Mining Sciences 34 (7), 1055 – 1064.

Thiemeyer, N., Habersetzer, J., Peinl, M., Zulauf, G., Hammer, J., 2015. The application of high resolution x-ray computed tomography on naturally deformed rock salt: Multi-scale investigations of the structural inventory. Journal of Structural Geology 77, 92–106.

Thiemeyer, N., Zulauf, G., Mertineit, M., Linckens, J., Pusch, M., Hammer, J., 2016. Microfabrics and 3d grain shape of gorleben rock salt: Constraints on deformation mechanisms and paleodifferential stress. Tectonophysics 676, 1 – 19.

Tijani, M., Apr. 2008. Contribution à l'étude thermomécanique des cavités réalisées par lessivage dans des formations géologiques salines. Habilitation à diriger des recherches, Université Pierre et Marie Curie - Paris VI.

Tijani, M., Vouille, G., Hugout, B., 1983. Le sel gemme en tant que liquide visqueux. In: Le sel gemme en tant que liquide visqueux. Melbourne, Australia, pp. 241–246.

Tsang, C.-F., Bernier, F., Davies, C., 2005. Geohydromechanical processes in the excavation damaged zone in crystalline rock, rock salt, and indurated and plastic clays—in the context of radioactive waste disposal. International Journal of Rock Mechanics and Mining Sciences 42 (1), 109 – 125.

Ulusay, R., Hudson, J., for Rock Mechanics. Commission on Testing Methods, I. S., 2007. The Complete ISRM Suggested Methods for Rock Characterization, Testing and Monitoring: 1974-2006. International Society for Rock Mechanics, Commission on Testing Methods.

Van-Hasselt, B., 12 1991. Évaluation qualitative du rôle de la texture dans le fluage du sel bressan. Ph.D. thesis.

509 Wang, T., Li, J., Jing, G., Zhang, Q., Yang, C., Daemen, J., 2019. Determination of the maximum allowable gas
510 pressure for an underground gas storage salt cavern – a case study of jintan, china. Journal of Rock Mechanics and
511 Geotechnical Engineering 11 (2), 251 – 262.
512 Wang, T., Yang, C., Chen, J., Daemen, J., 2018. Geomechanical investigation of roof failure of china's first gas storage
513 salt cavern. Engineering Geology 243, 59 – 69.
514 Wawersik, W. R., Hannum, D. W., 1980. Mechanical behavior of new mexico rock salt in triaxial compression up to
515 200c. Journal of Geophysical Research: Solid Earth 85 (B2), 891–900.

Effect of insoluble materials on the volumetric behavior of rock salt

M. Azabou[a,*], A. Rouabhi[a], L. Blanco-Martín[a]

[a]*MINES ParisTech, PSL Research University, Centre de Géosciences, 35 rue St Honoré 77300 Fontainebleau, France*

Abstract

This paper focuses on the presence of nodules of insoluble materials within salt specimens, and their effect on the volumetric strain measurements and the dilatancy phenomenon. We analyzed experimental results of over 120 conventional triaxial compression tests, and found that in 20% of the cases the volumetric strain measurements were atypical. We also noted that the natural variability of the specimens can lead to a non negligible data scattering in the volumetric strain measurements, when different specimens are subjected to the same test. This is expected given the small magnitude of those strains, but it occasionally implies that the corresponding specimens are not representative of the volumetric behavior of the studied rock. In order to understand these results, we conducted numerical investigations in which salt specimens are modeled as halite matrices with inclusions of impurities. Simulations of triaxial compression tests on these structures proved that such heterogeneities can induce dilatancy: their presence led to the appearance of tensile zones which is physically translated into a micro-cracking activity. The modeling approach was validated as the patterns displayed in the numerical results were identical to what is seen in the laboratory. It was then employed to provide an explanation to the observed irregularities in experimental results. We studied the natural variability effect as well and proposed a methodology to overcome the issue of specimens representativity from both deviatoric and volumetric perspectives.

Keywords: rock salt, dilatancy, material heterogeneity, natural variability, triaxial tests, virtual laboratory

1. Introduction

Solution mined cavities in salt formations have been used for hydrocarbon storage for about 70 years (Bays, 1963). What made this technique conceivable in the first place is the excellent sealing capacity of rock salt due to its naturally low porosity and permeability (Popp and Kern, 1998; Wang et al., 2019). However, underground cavity opening in undisturbed rocks results in the creation of disturbed zones around the underground facility (DeVries et al., 2002, 2005; Habibi, 2019), where the stress state is far from being isotropic and can present high levels of deviatoric stress (DeVries et al., 2002; Tsang et al., 2005).

Laboratory tests on salt specimens have proven that, under compressive loading and above some level of deviatoric stress, rock salt can undergo an irreversible volume increase resulting from a micro-cracking activity (DeVries et al., 2005). This phenomenon is known as dilatancy and is associated with material damage since the micro-cracking activity weakens the material and allows the development of flow paths (Stormont, 1997; Schulze et al., 2001; DeVries et al., 2002). Figure 1 shows the dilatancy onset during a triaxial test conducted under a confining pressure of 4 MPa and a constant axial strain rate of 5×10^{-5} s^{-1}.

*Corresponding author
Email address: mejda.azabou@mines-paristech.fr (M. Azabou)

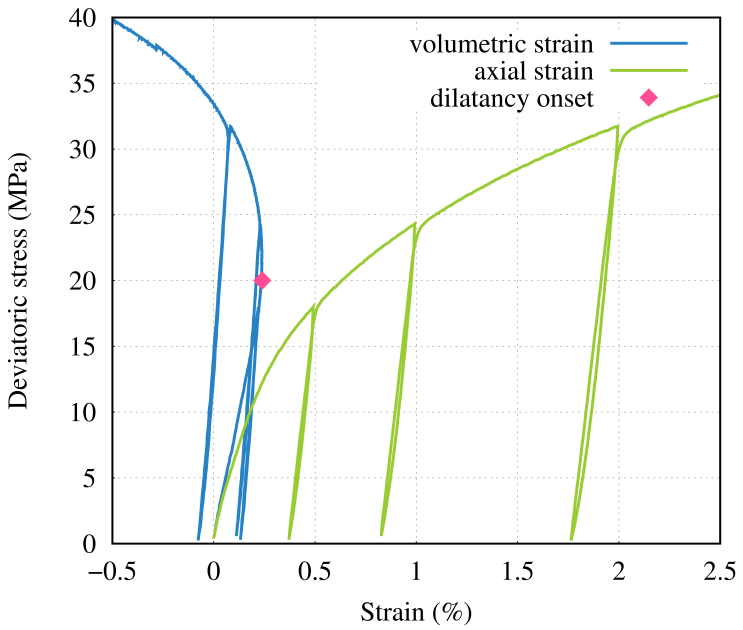

Figure 1: Experimental data of a triaxial compression test on a rock salt specimen (test conducted at Mines ParisTech). Compressive strains are positive.

Due to the stress state distribution around the cavity, dilatancy is likely to occur, compromising the integrity of the facility (DeVries et al., 2002; Wang et al., 2018; Labaune, 2018), hence the importance of the experimental measurements of volumetric strain. However, rock salt dilatancy usually occurs at small volumetric strains (typically below 0.4% (Roberts et al., 2015; Labaune, 2018; Rouabhi et al., 2019)), which is so small that rock salt viscoplastic deformation was considered isochoric for years (Munson and Dawson, 1981; Tijani et al., 1983; Heusermann et al., 2003). Thus, getting the accurate data is a delicate task as factors like natural variability, specimen heterogeneity, testing procedure or the used measurement techniques can significantly impact the results. Studies on factors influencing the volumetric strain measurements have been carried out: Medina-Cetina and Rechenmacher (2009); DeVries and Mellegard (2010) investigated the effect of specimens preconditioning; Hou (2003); DeVries et al. (2005); Rouabhi et al. (2019) tackled the effect of aspects of the loading conditions, and the measurement techniques effect was studied in Rouabhi et al. (2019).

Natural variability is an inevitable bias since we are studying a geological material. As will be

shown throughout this paper, the natural variability of the specimens has a slight effect on the deviatoric behavior; the exhibited dispersion in axial strain measurements remains within the ranges of measurements errors. However, regarding the volumetric ones, and due to their small magnitude as already mentioned, the measured volumetric behavior can show a non negligible dispersion. And this means that the used specimens could be non representative of the corresponding rock salt on the volumetric level albeit they are so from a deviatoric point of view.

The work of Rouabhi et al. (2019) and further illustrations throughout this paper show that if we exclude the dysfunction of the measurement techniques, volumetric strain data given by different measurement techniques can exhibit differences that cannot be attributed to the testing conditions alone. This raises questions concerning the material heterogeneity as it can lead to spatial heterogeneities in the stress and strain fields.

There are numerous aspects of material heterogeneity, they can be microscopic, i.e., related to the shape, size and orientation of the grains, related to fluid inclusions in grain boundaries or to the type of halite crystals (see Chemin, 1990; Van-Hasselt, 1991; Speranza et al., 2016, and references therein), as they can be macroscopic and visible on the specimen like the presence of nodules of anhydrite or clay, or even fracture plans. More details into the microscopic and macroscopic aspects of natural heterogeneity in rock salt can be found in the work of Speranza et al. (2016) and the references therein. The impurities present in rock salt are usually clay, anhydrite and marl Gillhaus et al. (2006). Their mass fraction is usually determined in the process of site characterization. It is a property that varies from one rock salt to another over a large range: in the Tersanne cavern field in south eastern France, the mass fraction of impurities in the salt formation is less than 10%, while in other formations this fraction can be greater than 50% (the Vauvert cavern field in south France).

To the best of the authors' knowledge, no studies have been carried out to investigate neither the effect of natural variability nor the impact of a specimen's spatial heterogeneity on the volumetric strain measurements, especially since they are used to determine design criteria for salt caverns.

The main purpose of this paper is to understand the effect of material heterogeneity on the experimental measurements of volumetric strain and to propose a methodology to overcome the issue of specimens representativity from a volumetric perspective. We chose to focus our work on the

presence of macroscopic nodules of insoluble materials within a supposedly pure halite matrix. Experimentally, investigating such factors is a delicate task as it requires precise data and cannot tolerate measurement errors and perturbations that are difficult to quantify. For this reason, we support our experimental investigation by an extensive numerical study. The use of a virtual laboratory will allow a better understanding of what is observed in the lab and will offer a ground to investigate the dilatancy phenomenon with a structural approach without the limitations of experimental works.

We mainly found that the dilatancy phenomenon could be a consequence of material heterogeneity and that the presence of insoluble materials can explain some of the atypical observations in the lab. We also showed how sensitive the volumetric strain measurements are to the natural variability of the specimens and proposed a methodology to overcome the issue of non representativity.

This paper is structured as follows. Section 2 is an experimental investigation that is focused on the volumetric strain measurements. Section 3 briefly presents the constitutive model used in the numerical study of section 4 during which the effect of heterogeneities on the volumetric behavior is investigated. This study is purely mechanical, neither the thermal nor the hydraulic aspects were taken into account.

2. Experimental data

We analyzed 11 experimental campaigns conducted at the Geosciences Department of Mines ParisTech on salt specimens from different locations in France and in the US between 2004 and 2012. Each testing program is comprised of conventional uniaxial and triaxial compression tests and creep tests. As volumetric strain measurements are only provided in triaxial compression tests, we focused our analysis on those experiments and the total number of studied tests was about 123. The tested specimens are 13 cm high cylinders with a slenderness ratio of 2. A triaxial compression test consists in maintaining a constant confining pressure on the lateral surface of the specimen by injecting/withdrawing a confining fluid into a triaxial cell, while imposing a constant axial strain rate via loading platens between which the specimen is placed (Wawersik and Hannum, 1980; Mellegard et al., 2005; Ulusay et al., 2007).

We distinguish two kinds of measurement techniques; "local" and "global". The local measure-

ments are given by strain gauges (axial and circumferential) placed at mid height of the specimen. The global measurements use an LVDT (linear variable displacement transducer) sensor attached to the loading platens and the amount of fluid injected or withdrawn from the cell (Rouabhi et al., 2019). Thus for the axial strain, the local measurement is given by the axial strain gauge and the global one is given by the LVDT sensor. The measurements of the axial and circumferential gauges are combined to get the local volumetric strain measurement whereas the axial displacement between the loading platens (measured by the LVDT) is combined with the amount of fluid injected or withdrawn from the cell to get the global volumetric strain measurement.

In the following, let Q be the applied axial stress, P the confining pressure, $|Q - P|$ the deviatoric stress and ζ the volumetric strain defined as:

$$\begin{cases} \zeta_g = -(V - V_i)/V_i \\ \zeta_l = -(2\varepsilon_\theta + \varepsilon_z) \end{cases} \tag{1}$$

where the subscripts g, l and i stand respectively for global, local and initial. The volume of the specimen is V, ε_θ and ε_z are the tangential and axial strains, respectively. Refer to Rouabhi et al. (2019) and references therein for further details on the given definitions.

2.1. Results and observations

The analysis of the experimental data and the examination of the corresponding specimens showed that in about 80% of the tests, the difference between the local and global measurements of axial strain is small and stays within the range of the uncertainty of the measurement techniques. Regarding the volumetric strain, there is always a difference between global and local measurements as the strain gauges measure dilatancy onset before it is seen by the whole specimen, i.e, before the global measurement indicates it. In these classic cases, the dispersion between local and global measurements is in the range of what is seen in the tests presented in the work of Rouabhi et al. (2019). Figure 2 shows the results of a typical test conducted under a constant strain rate of 5×10^{-5} s^{-1} and a confining pressure of 12 MPa. In this figure, the evolution of the deviatoric stress is presented as a function of global and local measurements of the axial and volumetric strains. As it can be seen, the dilatancy onset given by the global technique is about 2 times higher than the

one measured by the gauges, and this is a ratio that is seen in a large majority of the tests. On the other hand, the axial strain measurements present an acceptable dispersion.

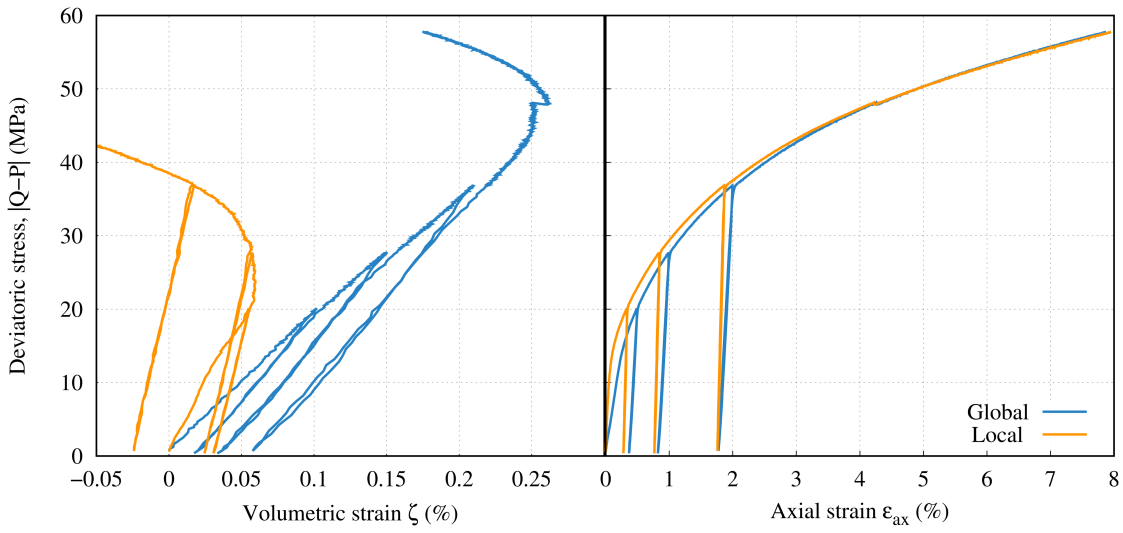

Figure 2: Results of a conventional triaxial compression test (P=12 MPa, $\dot{\varepsilon}_{ax} = 5 \times 10^{-5}$ s^{-1}) representative of 80% of the tests performed.

Regarding the remaining 20% of the tests, the local volumetric strain measurements are atypical and their comparison with the global ones is out of the pattern described for 80% of the tests. In these tests, we have cases where gauges indicate a higher deviatoric stress for dilatancy onset than what the global technique indicates. We also see cases where the gauges measure only contractancy or dilatancy during the entire test period whereas the global technique shows that the specimen undergoes contractancy and then dilatancy. Figures 3 to 6 give examples of these atypical observations and show the corresponding specimens as well. In Figure 3 the deviatoric stress corresponding to the global dilatancy onset is 8 times higher than the one measured by the local technique. Figure 4 indicates that when the deviatoric stress ranges between 35 and 50 MPa, the specimen undergoes a global increase in volume and a local contractancy at the same time. Figures 5 and 6 show that the local and global volumetric behaviors are significantly different during each of these tests.

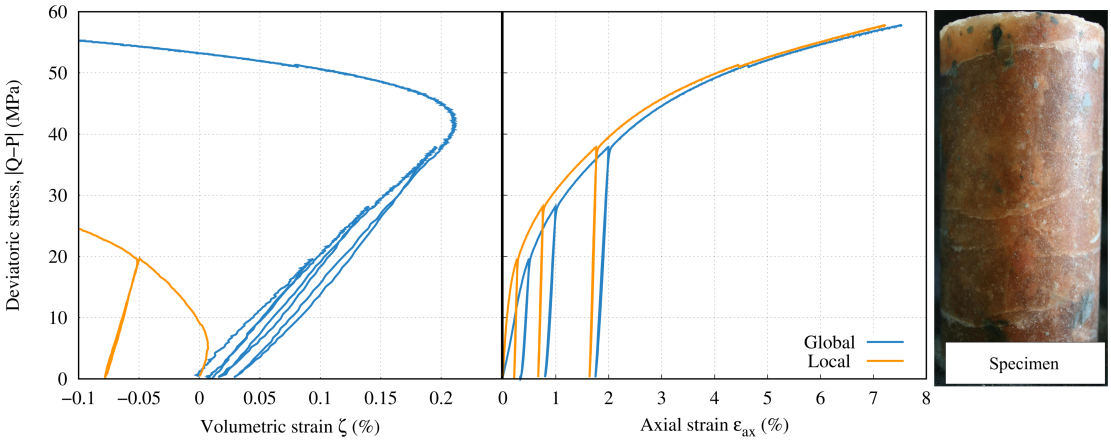

Figure 3: Results of a triaxial compression test (P= 12 MPa, $\dot{\varepsilon}_{ax} = 5 \times 10^{-5}$ s^{-1}) and the corresponding tested salt specimen, an example of the irregularities observed in 20% of the performed tests.

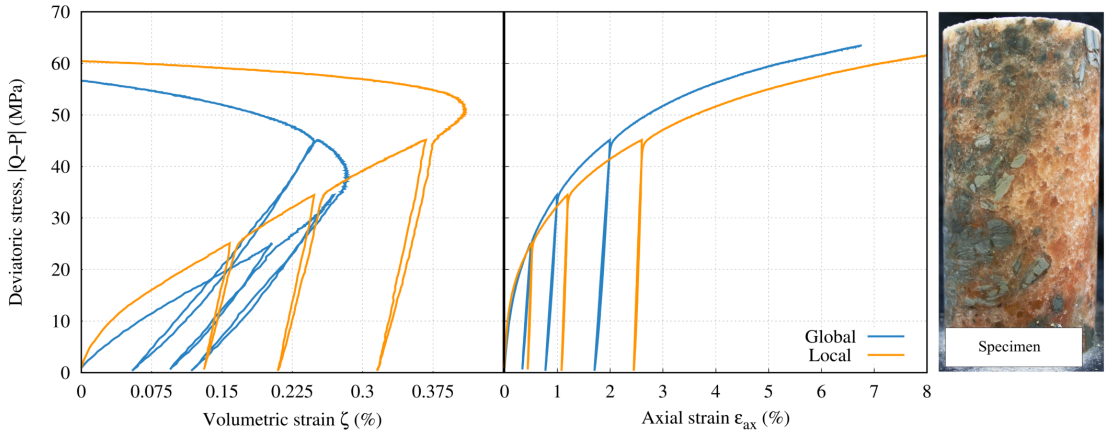

Figure 4: Results of a triaxial compression test (P= 12 MPa, $\dot{\varepsilon}_{ax} = 5 \times 10^{-5}$ s^{-1}) and the corresponding tested salt specimen, an example of the irregularities observed in 20% of the performed tests.

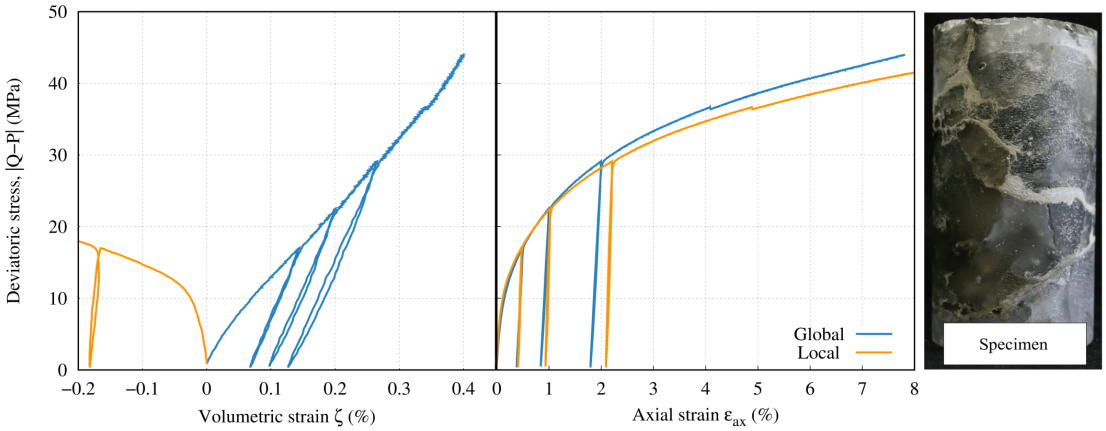

Figure 5: Results of a triaxial compression test (P= 12 MPa, $\dot{\varepsilon}_{ax} = 5 \times 10^{-5}$ s^{-1}) and the corresponding tested salt specimen, an example of the irregularities observed in 20% of the performed tests.

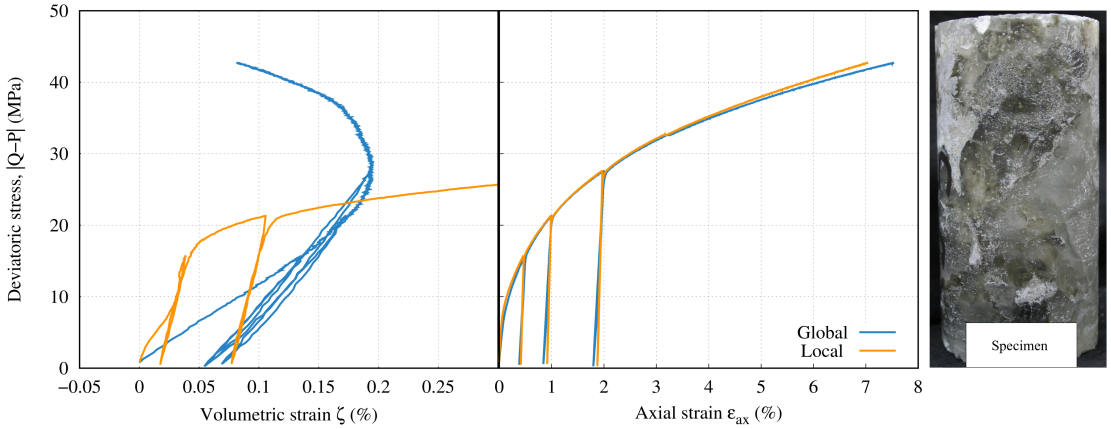

Figure 6: Results of a triaxial compression test (P= 8 MPa, $\dot{\varepsilon}_{ax} = 5 \times 10^{-5}$ s^{-1}) and the corresponding tested salt specimen, an example of the irregularities observed in 20% of the performed tests.

We have also studied the cases where the same test is conducted on two specimens in order to see to which extent could the natural variability affect the results and whether the resulting dispersion is acceptable. We observed that the natural variability does not have a significant effect on the axial strain, be it local or global, but it could significantly affect the volumetric behavior measurements. In Figures 7 to 9, we show 3 of these comparisons along with the concerned specimens.

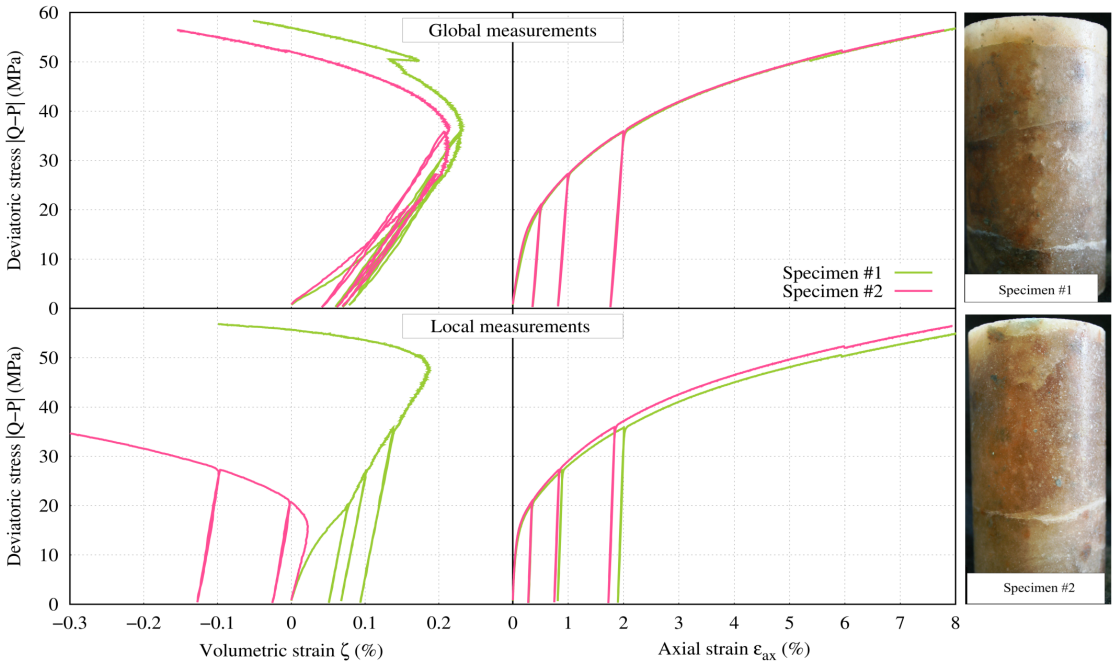

Figure 7: Results of two identical triaxial compression tests (P= 8 MPa, $\dot{\varepsilon}_{ax} = 5 \times 10^{-5}$ s^{-1}) and the corresponding tested salt specimens with difference in depths of 2.25 m.

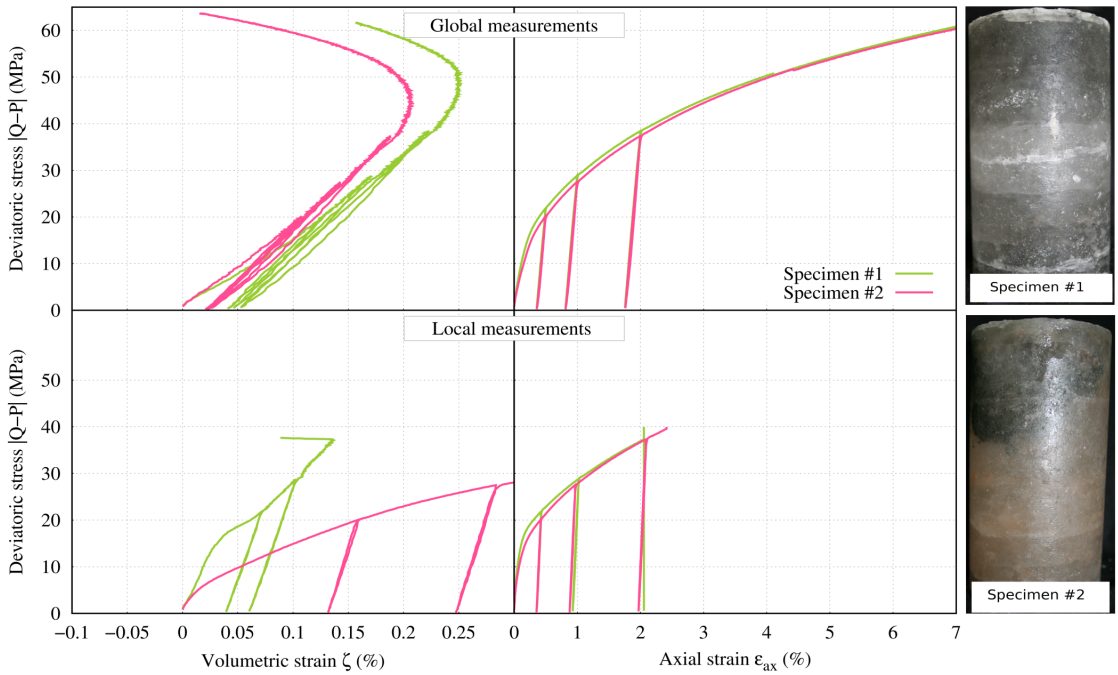

Figure 8: Results of two identical triaxial compression tests (P= 12 MPa, $\dot{\varepsilon}_{ax} = 5 \times 10^{-5}$ s^{-1}) and the corresponding tested salt specimens with difference in depths of 2.3 m.

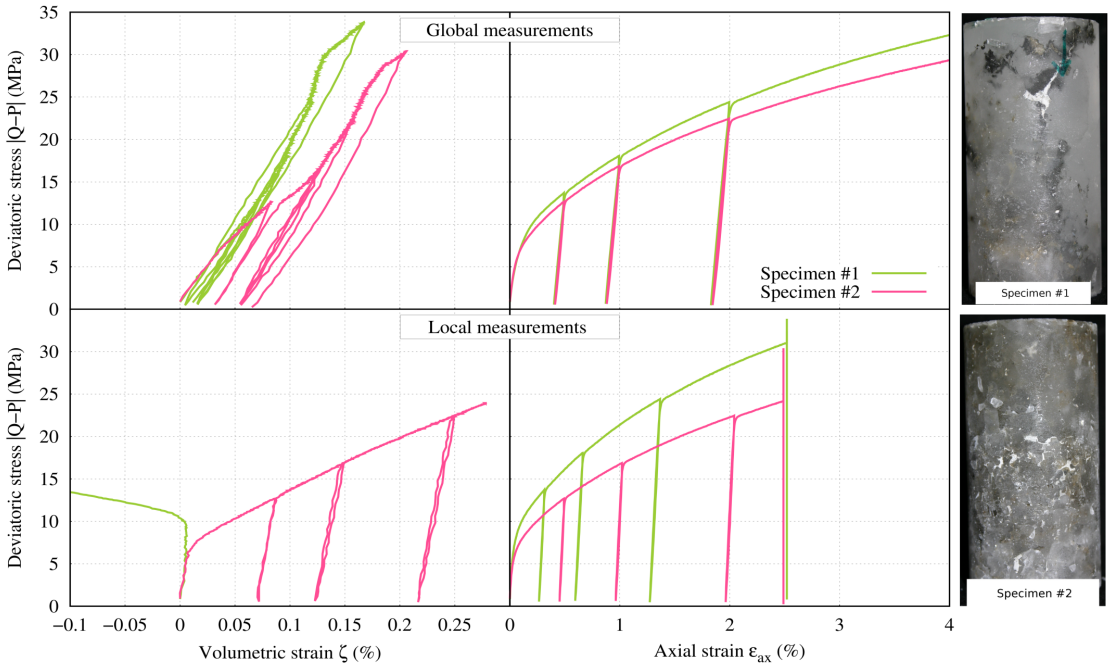

Figure 9: Results of two identical triaxial compression tests (P= 10 MPa, $\dot{\varepsilon}_{ax} = 2 \times 10^{-5}$ s^{-1}) and the corresponding tested salt specimens with difference in depths of 21.4 m.

2.2. *Discussion*

The analysis of these experimental data showed that it is possible for a specimen to display a local response that is significantly different from the global one. The malfunction of the measurement techniques is excluded: we have analyzed the results and confirmed that the gauges have been fully functional, we also assume that there were no oil leaks to alter the global measurement. Rouabhi et al. (2019) proved that the friction with the loading platens can in fact cause the local measurements to deviate from the global ones but not to the observed extent. This can be interpreted by the presence of material heterogeneity close to the placement of the gauges which capture very local phenomena due to their size.

We have also seen that specimens that are considered representative of a given rock salt, can show a very similar deviatoric behavior when subjected to the same loading conditions but a different volumetric behavior: the dispersion is always more pronounced in the local measurements. This implies that, especially in terms of the volumetric response, our specimens could be smaller than the required representative element volume (REV) for the studied rock salt.

Both of these observations can be traced back to the material spatial heterogeneity and among the many aspects of it (Chemin, 1990; Van-Hasselt, 1991; Thiemeyer et al., 2015; Speranza et al., 2016; Thiemeyer et al., 2016; Mansouri et al., 2019), we chose to focus this study on the presence of nodules of impurities similar to what can be seen on the specimen from Figure 4.
We investigate the effect of such heterogeneity on the volumetric behavior and the representativity of the used specimens. Rigorous experimental investigation of this aspect is problematic due to the following reasons:

- we do not have control over the material heterogeneity; as it was mentioned before, various aspects of heterogeneity exist within a salt sample which means that we cannot attribute a certain behavior to one particular aspect;

- the measured volumetric strains are extremely small (Roberts et al., 2015; Labaune, 2018; Rouabhi et al., 2019) which means the errors and uncertainties inherent to the laboratory work can be non negligible and can affect the measurements and therefore alter our interpretations and analysis;

- in order to further investigate the representativity of the specimens, we need to perform typical triaxial compression tests on bigger samples. This is often complicated due to the limitations of the experimental facilities: typically a lab is equipped with cells that can host specimens heaving at most 2 or 3 particular diameters (respecting the dimensions specified in Ulusay et al. (2007)), and it is unrealistic to have a new cell each time there is a need to characterize a different rock.

Consequently, we decided to use a virtual laboratory built on numerical modeling and simulation tools. This will allow to investigate the effect of this particular aspect of heterogeneity on rock salt dilatancy in an attempt to understand the mentioned observations.

3. Constitutive model

This model has been developed by Rouabhi et al. (2019). It assumes an additive decomposition of the total strain rate tensor $\underline{\underline{\dot{\varepsilon}}}_{vp}$ into tensile $\underline{\underline{\dot{\varepsilon}}}^{t}_{vp}$ and compressive $\underline{\underline{\dot{\varepsilon}}}^{c}_{vp}$ parts.
The compressive and tensile parts of the viscoplastic strain rate tensor $\underline{\underline{\dot{\varepsilon}}}_{vp}$ are decomposed in the basis $(\underline{\underline{I}}, \underline{\underline{J}}, \underline{\underline{K}})$ defined as

$$\underline{\underline{I}} = \underline{\underline{1}}/\sqrt{3}, \quad \underline{\underline{J}} = \underline{\underline{\sigma}}'/\|\underline{\underline{\sigma}}'\|, \quad \underline{\underline{K}} = (\sqrt{2}\underline{\underline{I}} + \ell\underline{\underline{J}} - \sqrt{6}\underline{\underline{J}}^2)/\sqrt{1-\ell^2} \tag{2}$$

where $\underline{\underline{\sigma}}'$ is the deviatoric part of the stress tensor $\underline{\underline{\sigma}}$; and $\ell = \sqrt{6}tr(\underline{\underline{J}}^3)$ is the third invariant of $\underline{\underline{\sigma}}'$.
Under compressive loading, the evolution law of $\underline{\underline{\dot{\varepsilon}}}^{c}_{vp}$ can be written as

$$\underline{\underline{\dot{\varepsilon}}}^{c}_{vp} = -\sqrt{1/3}\dot{\zeta}^{c}_{vp}\underline{\underline{I}} + \sqrt{3/2}\dot{\gamma}^{c}_{vp}\underline{\underline{N}}^{c} \tag{3}$$

where $\dot{\zeta}^{c}_{vp} = -tr(\underline{\underline{\dot{\varepsilon}}}^{c}_{vp})$ and $\dot{\gamma}^{c}_{vp} = \sqrt{2/3}\|\underline{\underline{\varepsilon}}^{c}_{vp}{}'\|$ are the rates of the volumetric strain and the viscoplastic distorsion, respectively and $\underline{\underline{N}}^{c}$ is a unit tensor defining the deviatoric flow direction under compressive loading.
Under tensile loading, the strain rate tensor $\underline{\underline{\dot{\varepsilon}}}^{t}_{vp}$ is assumed to be described by a mechanism of Rankine-type:

$$\underline{\underline{\dot{\varepsilon}}}^{t}_{vp} = \dot{\lambda}\frac{\partial G}{\partial \underline{\underline{\sigma}}} \tag{4}$$

with

$$G = (\langle\sigma_1\rangle^d + \langle\sigma_2\rangle^d + \langle\sigma_3\rangle^d)^{1/d} \tag{5}$$

where $\dot{\lambda}$ is a positive multiplier, $\langle.\rangle$ are the Macaulay brackets, i.e. $\langle x\rangle = (x+|x|)/2$; $\sigma_1 \geq \sigma_2 \geq \sigma_3$ are the principal stresses of $\underline{\underline{\sigma}}$; and $d \geq 1$ is a constant parameter.
When the gradient of G with respect to $\underline{\underline{\sigma}}$ is written in the basis $(\underline{\underline{I}}, \underline{\underline{J}}, \underline{\underline{K}})$, Equation 4 can be rewritten as:

$$\underline{\underline{\dot{\varepsilon}}}^{t}_{vp} = -\sqrt{1/3}\dot{\zeta}^{t}_{vp}\underline{\underline{I}} + \sqrt{3/2}\dot{\gamma}^{t}_{vp}\underline{\underline{N}}^{t} \tag{6}$$

with

$$\dot{\zeta}^{t}_{vp} = -\dot{\lambda}X, \quad \dot{\gamma}^{t}_{vp} = \dot{\lambda}\sqrt{Y^2 + Z^2} \tag{7}$$

where $\underline{\underline{N}}^t$ defines the deviatoric flow direction under tensile loading and the quantities X, Y and Z are such that

$$\begin{cases} X = G'_1 + G'_2 + G'_3 \\ Y = (2G'_1 - G'_2 - G'_3)/3 \\ Z = (G'_2 - G'_3)/\sqrt{3} \end{cases} \tag{8}$$

with $G'_i = \langle \sigma_i / G \rangle^{d-1}$ the eigenvalues of $\partial G / \partial \underline{\underline{\sigma}}$.

Finally, the additive decomposition of the total strain rate tensor $\underline{\underline{\dot{\varepsilon}}}_{vp}$ into tensile $\underline{\underline{\dot{\varepsilon}}}^t_{vp}$ and compressive $\underline{\underline{\dot{\varepsilon}}}^c_{vp}$ parts, leads to

$$\underline{\underline{\dot{\varepsilon}}}_{vp} = -\sqrt{1/3}\dot{\zeta}_{vp}\underline{\underline{I}} + \sqrt{3/2}\left(\dot{\gamma}^c_{vp}\underline{\underline{N}}^c + \dot{\gamma}^t_{vp}\underline{\underline{N}}^t\right) \tag{9}$$

with $\dot{\zeta}_{vp} = \dot{\zeta}^c_{vp} + \dot{\zeta}^t_{vp}$. As can be seen from this Equation, the tensile contribution acts on both components of $\underline{\underline{\dot{\varepsilon}}}_{vp}$, volumetric and deviatoric.

To fully define $\underline{\underline{\dot{\varepsilon}}}_{vp}$, $\dot{\gamma}^c_{vp}$, $\dot{\zeta}^c_{vp}$ and $\dot{\lambda}$ need to be defined, which will be done as follows.

For the compressive part, the evolution law of $\dot{\zeta}^c_{vp}$ is expressed as

$$\dot{\zeta}^c_{vp} = \psi\left(\underline{\underline{\sigma}}, \gamma^c_{vp}\right)\dot{\gamma}^c_{vp} \tag{10}$$

with

$$\psi\left(\underline{\underline{\sigma}}, \gamma^c_{vp}\right) = z\frac{\left\langle p/N \right\rangle^n - \gamma^c_{vp}}{\left\langle p/M \right\rangle^m + \gamma^c_{vp}} \tag{11}$$

and γ^c_{vp} is given through a generalization of Lemaitre model (Tijani et al., 1983), enriched with an influence of the mean pressure p and the Lode angle θ:

$$\frac{d\left(\gamma^c_{vp}\right)^{1/a}}{dt} = \left\langle \left[q/\varrho(\theta) - \left(\gamma^c_{vp}\right)^b Bp - C \right] \Big/ K \right\rangle^{k/a} \tag{12}$$

In Equation 11, the sign of $\langle p/N \rangle^n - \gamma^c_{vp}$ indicates whether the behavior is contracting or dilating.

Regarding the tensile part, we consider an evolution law of Perzyna-type:

$$\dot{\lambda} = \Lambda \langle (G - R_t)/S \rangle^s \tag{13}$$

In Equations 11 to 13, $z, n, m, a, b, B, C, K, k, \Lambda, R_t, d, s, M, N$ and S are the material parameters. When this model is used to simulate a triaxial compression test, dilatancy is:

- taken into account on a constitutive level when we assume that the stress field within the specimen is homogeneous and all stresses are compressive (Equations 10 and 11);
- a result of a heterogeneous distribution of the stress field leading to activating the tension mechanism (Equations 7 and 13).

4. Numerical Investigations

We first present and validate our numerical approach which is then employed to investigate the volumetric strains measured by different measurement techniques on a salt specimen containing nodules of impurities. The natural variability, its effect on the volumetric strain measurements and the specimens representativity are discussed in section 4.3.

4.1. Structural approach for dilatancy

The micro structure of a salt specimen in reality is very complex to be reproduced numerically (different grain sizes, fluid inclusions, grain boundaries, different types and shapes of heterogeneities,...). In this work, we assume that salt is a two-phase medium composed of a pure halite matrix and nodules of insoluble materials. This simplifying assumption is accepted, since the aim of this research is to qualitatively understand the impact of the presence of heterogeneities on the macroscopic behavior. Thus the numerical validation of the approach does not concern its ability to reproduce the complex geometry of real salt specimens, but rather the measurements of physical quantities.

A salt specimen is modeled as a cylindrical matrix of pure halite, with inclusions representing the nodules of insolubles as shown in Figure 10. The insolubles are modeled as spheres for the sake of simplicity and the specimens are generated as follows. First, a cube's side length, the volume fraction of insolubles within the cube, the minimum and maximum radii (of the inclusions) are designated. Second, an iterative process allows to generate, via a uniform random number generator, the position of a sphere center (within the cube) and a radius (between the specified bounds); the respect of the specified volume fraction is checked at each iteration. Finally, once the distribution of the spheres is generated within the cube, the position and size of the specimen to model are chosen and the virtual sampling is performed.

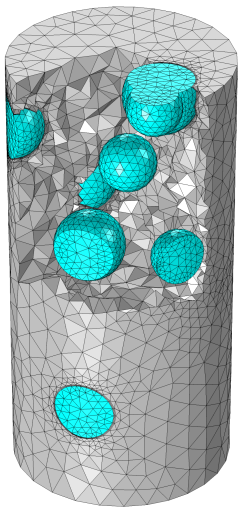

Figure 10: Cutaway view of the modeled structure of a salt specimen with nodules of insolubles.

The structure shown in Figure 10 will be used as a reference specimen for our numerical investigations. It contains a volume fraction of inclusions of $\phi = 10.3\%$, the density of the halite matrix is assumed to be 2160 kg/m^3 which leads to a mass fraction of $w = 8.3\%$. Such mass fraction is within the usual ranges found in salt rocks (Gillhaus et al., 2006). The insolubles are considered to have properties similar to clay: a density of $\rho = 1700$ kg/m^3, a Young's modulus of $E = 5000$ MPa and a Poisson's ratio of $\nu = 0.32$.

We assume the continuity of the displacement field within the structure, and we do not introduce a joint model for the interface halite-inclusions. This simplifying assumption was made because on one hand the joint parameters are difficult to determine experimentally and on the other hand, introducing additional parameters will further complicate the study especially with the meshing requirement of the modeled structures. The assumption is valid since, as will be shown through this paper, the macroscopic aspects of rock salt behavior are reproduced.

The behavior of the insolubles is assumed to be linear elastic while the salt matrix is governed by the constitutive law presented in section 3.The parameter set used for the salt matrix is presented in Table 1. This parameter set was adopted from Labaune (2018) where the distorsion and dilatancy parameters were obtained by fitting triaxial compression and creep tests, and fitting a Brazilian test provided the ones relative to the tension mechanism. In this work, some of these parameters

are changed. The tensile strength is set to $R_t = 0$ (Equation 13) in compliance with setting the cohesion $C = 0$ (Equation 12). Also, setting the parameter $B = 0$ (Equation 12) means that we omit the mean pressure effect and setting $z = 0$ (Equation 11) implies that the viscoplastic volumetric strain due to compressive stresses is not considered. The tensile part is deactivated by setting the parameter $\Lambda = 0$ (Equation 13).

Elasticity					
E	ν				
20000	0.32				
Distorsion					
a	k	b	B	K	C
0.29	2.2	0.24	0	0.13	0
Dilatancy					
z	n	N	m	M	
0	1.3	0.012	3.3	1.37	
Tension					
d	Λ	R_t	S	s	
10	0	0	1	1	

Table 1: Parameters used to simulate the behavior of the salt matrix. The unit system is such that strain is in μm/m, stress is in MPa and time in days.

We used VIPLEF3D, a finite element code developped in the Geosciences Department of Mines ParisTech(Tijani, 2008) to simulate a typical triaxial test on the structure shown in Figure 10. The simulated test is conducted under a constant strain rate of 10^{-6} s^{-1} and a confining pressure of 5 MPa.

The results showed that within the salt matrix and around the spherical inclusions, zones where the principal major stress σ_1 is positive appear and continue to develop all along the simulation. Figure 11 shows the distribution of σ_1 within the salt matrix at an axial strain $\varepsilon_{ax} \approx 2\%$: the difference in rigidity of the inclusions and the halite matrix led to the appearance of tensile zones and to stress concentrations.

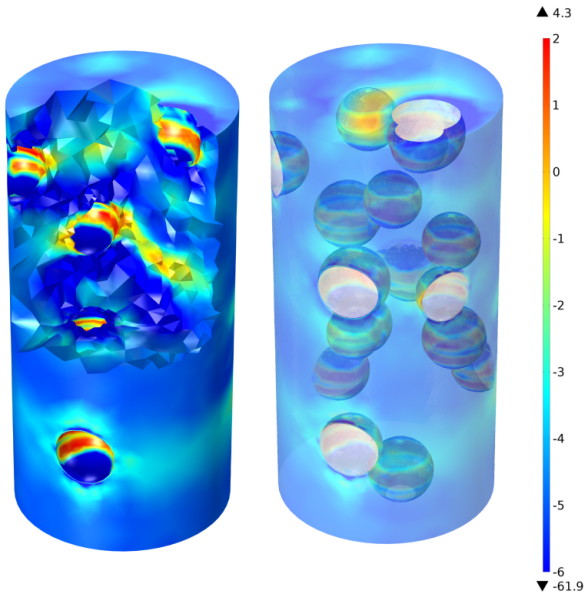

Figure 11: Cutaway (left) and transparent (right) views of the distribution of σ_1 (MPa) within the salt matrix at $\varepsilon_{ax} \approx 2\%$ (simulation of a typical triaxial compression test under a confinement of 5 MPa and an axial strain rate of 10^{-6} s^{-1}, on the specimen shown in Figure 10).

Because of these results, we re-conducted the same simulation except for activating the tensile part this time (the parameter Λ from Equation 13 was set to 5×10^4). Activating this component of the viscoplastic strain tensor means that in the halite matrix, irreversible strains are of two kinds: those governed by the deviatoric creep mechanism and those governed by the tensile mechanism, which obviously vanish under compressive loadings when the assumption of stress homogeneity usually made in the analysis of laboratory tests, is used.

The obtained results of the two performed simulations in terms of global measurements are given in Figure 12.

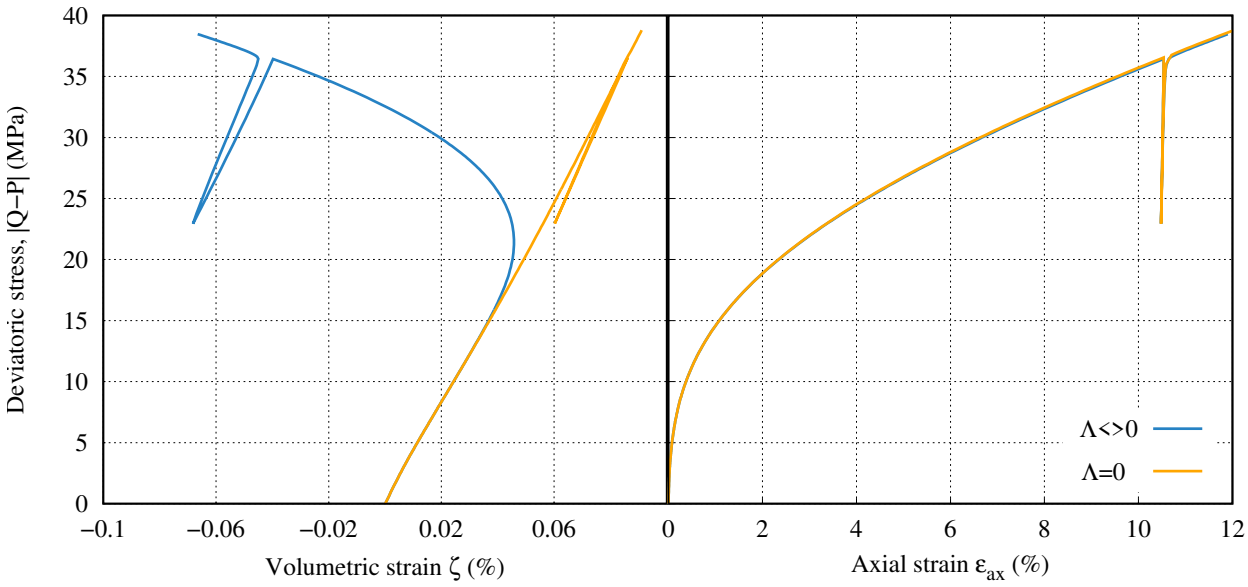

Figure 12: Results of simulations of a typical triaxial compression test under a confinement of 5 MPa and an axial strain rate of 10^{-6} s^{-1}, on the specimen shown in Figure 10.

The overall behavior of the structure has the same characteristics observed in the lab for salt specimens during this type of tests: viscoplastic hardening, contractancy and dilatancy. This is an important result because it shows that dilatancy can be a consequence of the material spatial heterogeneity. In fact in this study, the presence of heterogeneities lead to the development of stress concentrations and induced tensile stress zones which physically reflect the occurrence of a micro-cracking activity and therefore dilatancy. We still need to validate the ability of the approach to reproduce other characteristics like the mean pressure and the loading rate effects and most importantly the creep behavior. We use the reference specimen from Figure 10 to simulate a series of lab tests, as listed in Table 2.

Studied Aspect	$\dot{\varepsilon}_{ax}$ [s^{-1}]	P [MPa]	Stages of $\lvert Q-P\rvert$ [MPa]
Effect of loading rate	10^{-6}, 5×10^{-6}, 10^{-5}	5	-
Effect of the mean pressure	10^{-6}	0, 5, 10, 15	-
Creep behavior	-	5	5, 10

Table 2: Lab tests simulated on the specimen shown in Figure 10.

The results of these simulations are shown in Figures 14 to 15 and are considered very satisfactory as both effects of loading rate and mean pressure are correctly predicted. In fact, the dilatancy limit increases with the mean pressure (equivalent to confining pressure effect) and is significantly affected by the loading rate: the slower the test the lower the dilatancy limit (Labaune et al., 2018). Also the creep behavior is very similar to what is typically seen in the lab (Günther et al., 2015; Labaune et al., 2018).

These results have been obtained as well for other structures with different inclusions shape, distribution, size, volume fraction and different elastic constants. This approach is then assumed to be valid to describe rock salt behavior in the lab.

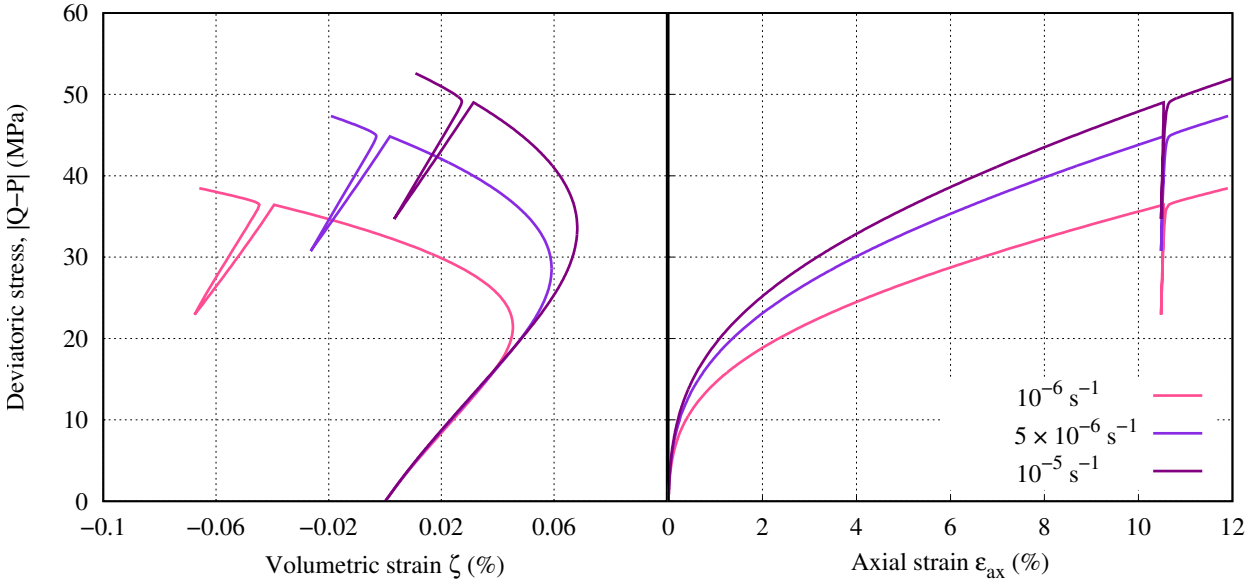

Figure 13: Results of simulations of typical triaxial tests (P=5 MPa) on the specimen in Figure 10 : effect of loading rate.

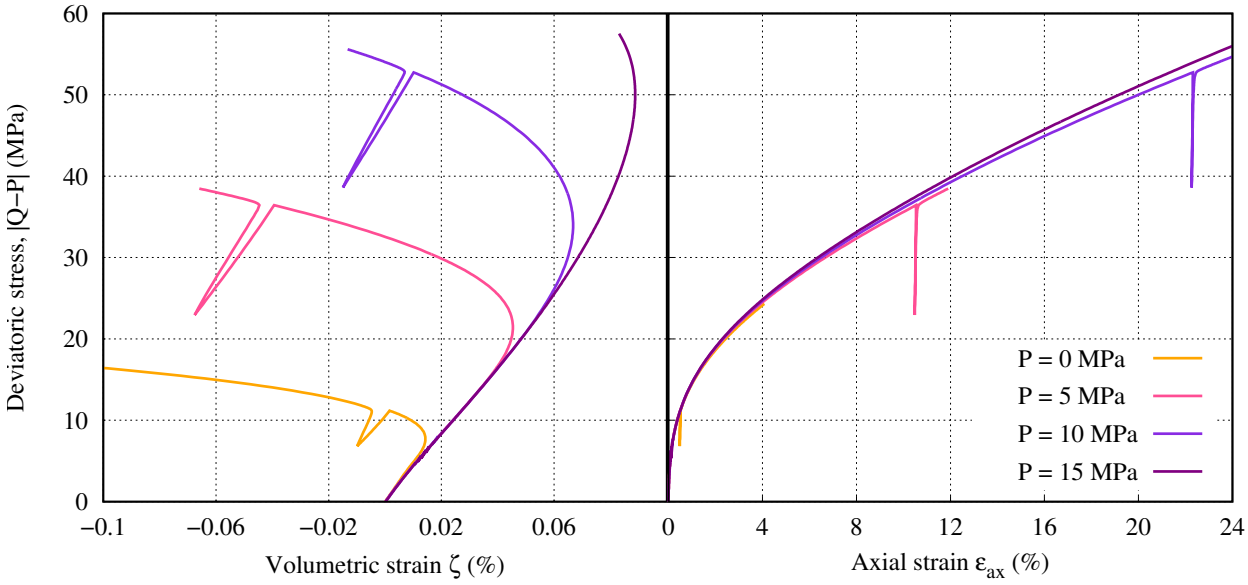

Figure 14: Results of simulations of typical triaxial tests ($\dot{\varepsilon}_{ax} = 10^{-6}$ s^{-1}) on the specimen in Figure 10 : effect of confining pressure.

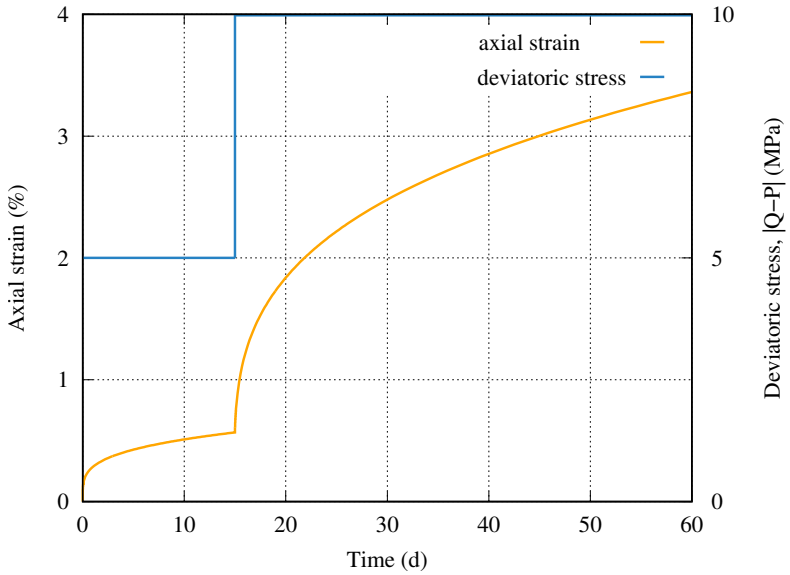

Figure 15: Results of a simulation of a typical triaxial multistage creep test (P=5 MPa) on the specimen in Figure 10.

4.2. Volumetric strain measurements on a heterogeneous specimen

We adopt the approach detailed in section 4.1 and the same parameter set given in Table 1 for the numerical study hereafter where we try to understand the experimental observations and obtain a qualitative assessment of the effect of heterogeneities on the volumetric behavior of rock salt. We simulated on the reference specimen in Figure 10, a conventional triaxial test under a confining pressure of 5 MPa and a constant axial strain rate of $10^{-6}s^{-1}$ (see Figure 13). We modeled the placement of two sets of strain gauges on the specimen in an attempt to get local strain measurements with the same procedure used in the lab. We have randomly chosen the position of the two sets of gauges, the only conditions were that the sets have to be placed at mid-height and on the salt matrix's lateral surface. We chose to investigate the effect of the friction with the platens as well so the simulation was conducted twice with the two extreme conditions of specimen-platen contact: smooth contact with no friction between the specimen and the loading platens and rough contact where there is a complete radial restraint on the specimen ends. This last boundary condition causes the initially right cylinder specimen to deform into a barrel (triaxial compression) or an hourglass (triaxial extension) shape (Labaune, 2018; Rouabhi et al., 2019). Figure 16 shows the obtained results.

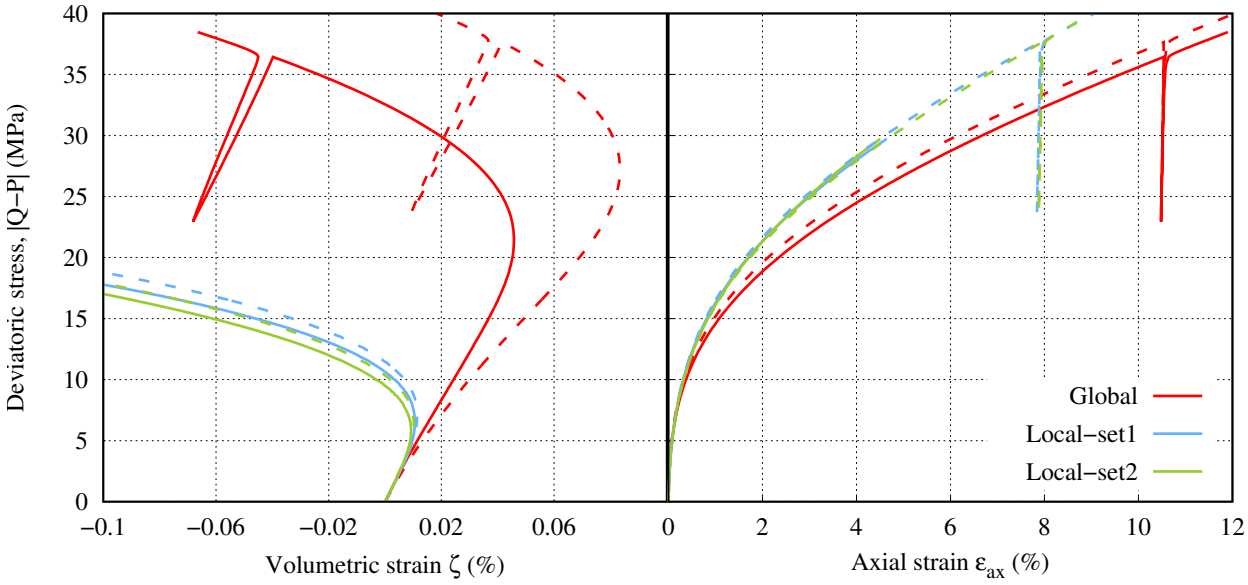

Figure 16: Results of a simulation of a typical triaxial compression test (P=5 MPa and $\dot{\varepsilon} = 10^{-6}$ s^{-1}) on the specimen in Figure 10. Curves in dashed and continuous lines correspond respectively to simulations with and without accounting for the friction with the loading platens.

These results show that the friction with the platens significantly affects the global volumetric strain measurements but it has a slight impact on the axial and the local volumetric strain measurements. The sets of gauges give very similar results in terms of both axial and volumetric strains, in fact this specimen does not have locations of inclusions concentration, instead the spheres are almost evenly distributed (see the transparent view in Figure 10). This leads to a sort of uniformity over the lateral surface : all gauges placed at mid-height of the specimen are likely to give very similar measurements; no gauge could be significantly more exposed to inclusions than others. We often have specimens were the inclusions are not evenly distributed as can be seen on the specimen in Figure 4: in this sample we can see that there are areas on the lateral surface that are covered with insolubles and others that are almost clear. To study such cases, we conduct the same simulation on the specimen presented in Figure 17. In this case, we placed the first set of gauges near the inclusion we see on the lateral surface of the specimen and the second set on the opposite side (relatively furthest from inclusions). The results are shown in Figure 17.

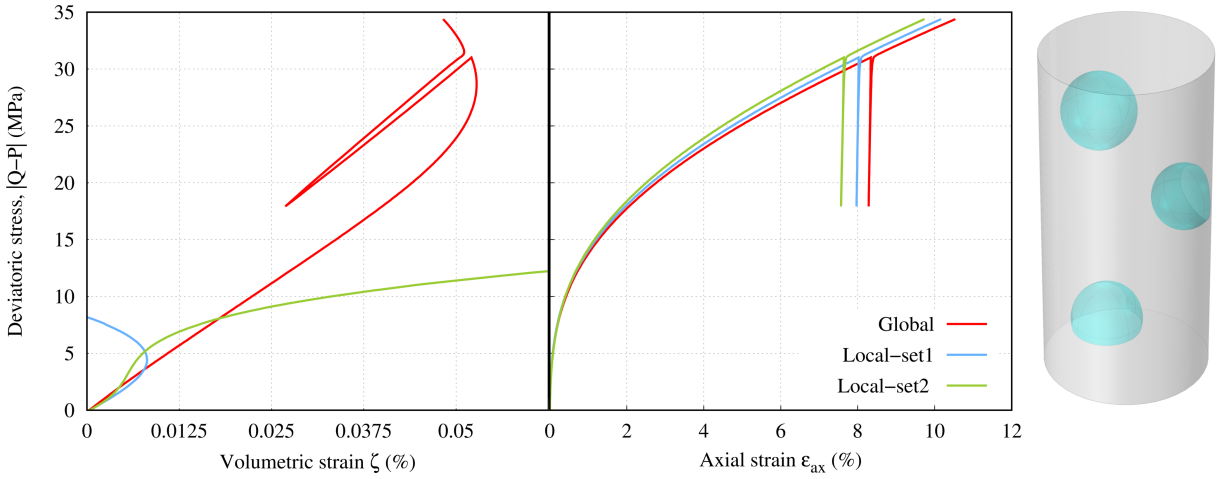

Figure 17: Results of a simulation of a typical triaxial compression test (P=5 MPa and $\dot{\varepsilon} = 10^{-6}$ s^{-1}) and the corresponding specimen.

We see similarly to what has been noted at the lab, the axial strain measurement is slightly affected, the dispersion shown between global and local measurements is acceptable. Regarding the volumetric strains, the difference is out of the usual ranges and patterns (see Figure 2). At a deviatoric stress level of ≈ 4 MPa, the first set (closest to the inclusions) measures significantly important radial strains due to the local appearance of tensile stresses (see Figure 11) and we see a local dilatancy onset. On the other hand, the second set (furthest from the inclusions) only sees contractancy until the end of the simulation: the radial strains in that location of the specimen were never important because tensile stresses did not appear there. It is not until the deviatoric stress reaches ≈ 27 MPa that the whole specimen's volume begins to increase. The information provided by the sets of gauges are true but have unexpected patterns and dilatancy onset values because they capture very local phenomena.

In this investigation we have provided a possible interpretation to cases like the ones presented in Figures 3 and 6. We have also given a possible explanation to one of the main conclusions of Rouabhi et al. (2019) which states that the friction with the loading platens cannot explain the difference observed between local and global measurements of the volumetric strain.

4.3. Natural Variability and Specimens Representativity

In this section, we investigate the representativity of specimens from a volumetric point of view. We generate a random distribution of spheres with radii ranging from 8 to 20 mm within $\approx 7\%$ of the volume of a 20 cm side length cube. As shown in Figure 18, we virtually sample this cube and generate 4 salt specimens that are 13 cm high with a diameter of 6.5 cm. The inclusions and the halite matrix have the properties mentioned in section 4.1. The mass fraction of insolubles in each specimen is indicated in Figure 18 as well.

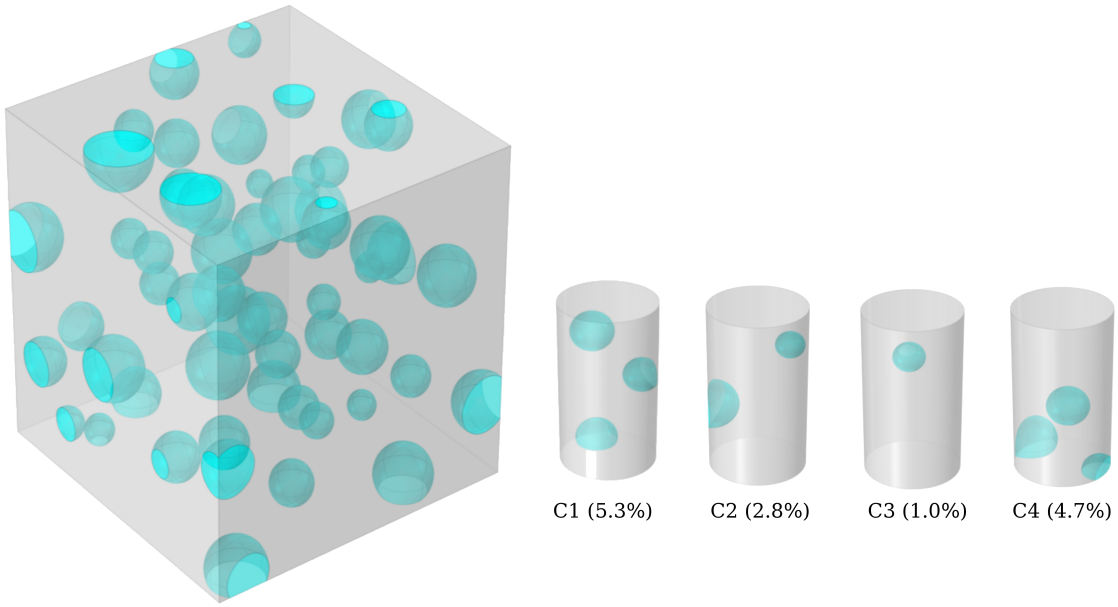

Figure 18: A modeled salt block with virtually sampled specimens, the mass fraction of insolubles is indicated for each specimen.

For each of the four shown specimens, we simulate a conventional triaxial compression test where the axial strain rate is fixed at $10^{-6}s^{-1}$ and the confining pressure at 5 MPa. The simulations continued until dilatancy onsets were globally seen. The results are shown in Figure 19 in terms of global measurements.

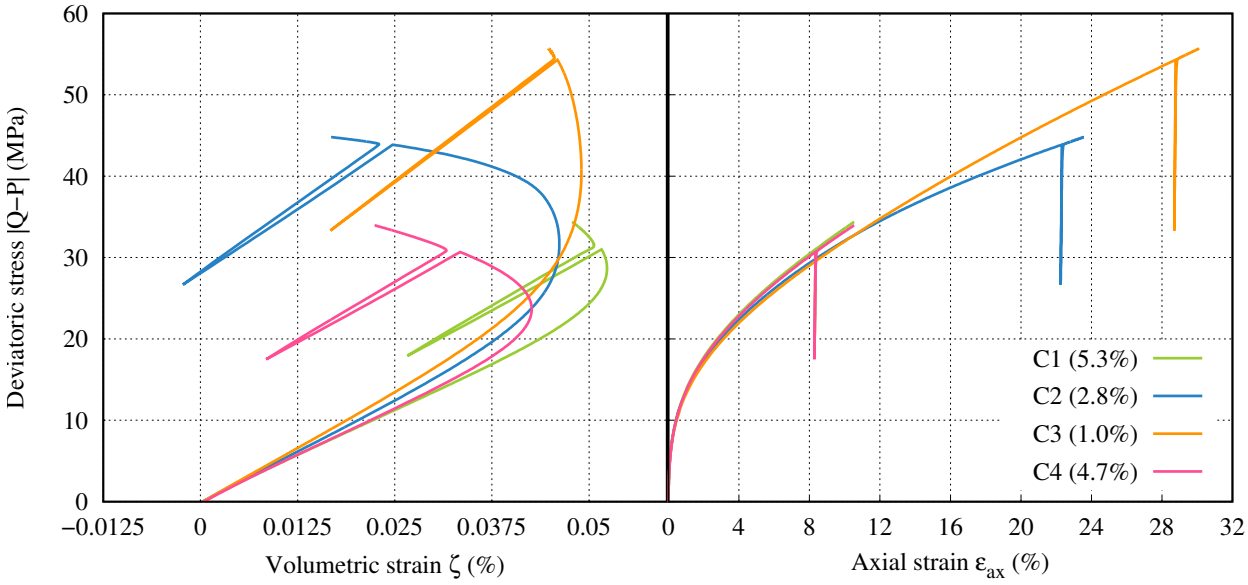

Figure 19: Results of a conventional triaxial compression test (P=5 MPa and $\dot{\varepsilon} = 10^{-6}$ s^{-1}), on the specimens shown in Figure 18.

As shown in Figure 19, the axial strain measurements present slight deviations, while the volumetric ones are significantly different. Because of the size of the insolubles and their distribution within the initial block, none of the sampled specimens were representative of the block from a volumetric perspective. Testing bigger specimens might seem like an immediate and ideal solution for this issue. However in practice, we may be constrained by the geometry of the available triaxial cells as explained in section 2 and we may even face cases where the maximum testable size (diameter equal to the coring diameter and a slenderness ratio of two) is not representative of the rock in question. Besides, testing bigger specimens is likely to compromise the precision of the obtained strain measurements; in fact the bigger the specimen, the bigger the required volume of confining oil and the less accurate the obtained volumetric strain measurements.

We study a second case scenario, where we generate a random distribution of spheres with radii ranging from 5 to 10 mm within $\approx 5\%$ of the volume of a 20 cm side length cube. As shown in Figure 20, we virtually sample this cube and generate 3 salt specimens that are 13 cm high with a diameter of 6.5 cm. Using the same properties for the inclusions and the halite matrix as the previous case, the mass fraction of insolubles in each specimen is indicated in Figure 20. We simulate

the same test as performed on the specimens shown in Figure 19 and we present the corresponding results in Figure 21.

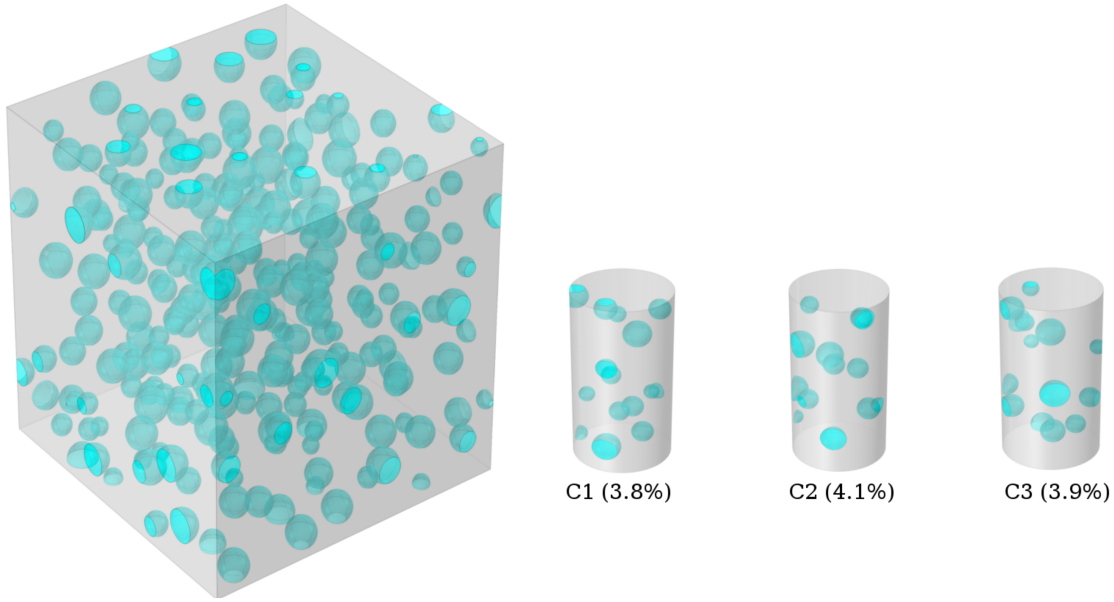

Figure 20: A modeled salt block with virtually sampled specimens, the mass fraction of insolubles is indicated for each specimen

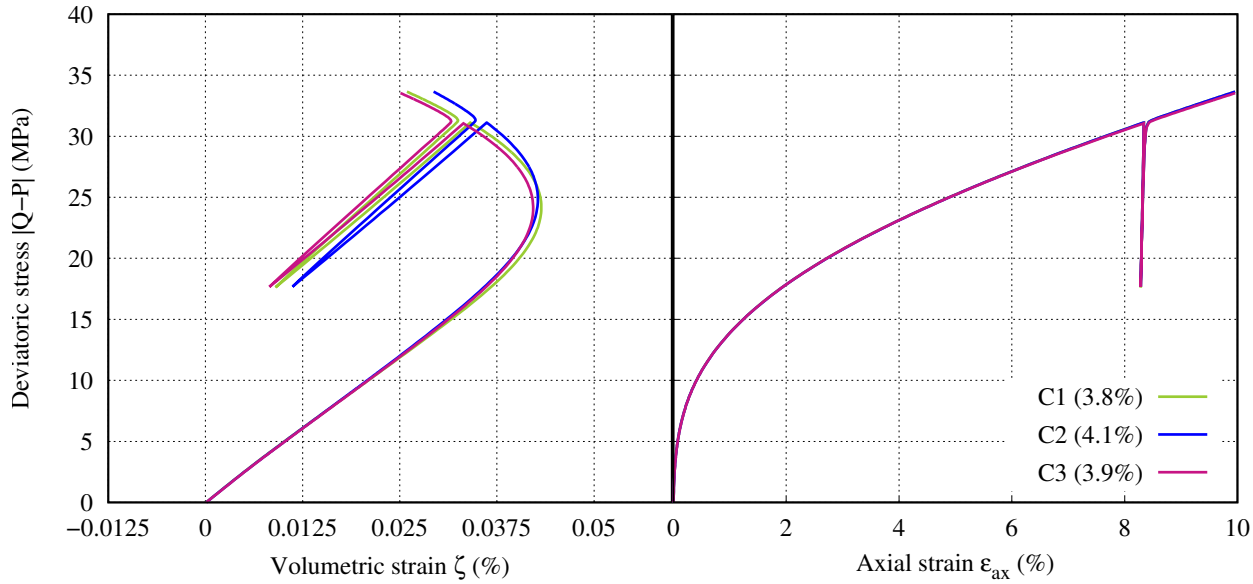

Figure 21: Results of a conventional triaxial compression test (P=5 MPa and $\dot{\varepsilon} = 10^{-6}$ s^{-1}), on the specimens shown in Figure 20.

In this case, the inclusions size is small compared to the dimensions of the specimen, in fact for all three of the cases we have $R_{max}/R_{spec} \approx 0.29$ where R_{max} is the radius of the largest sphere included within the halite matrix and R_{spec} is the radius of the specimen. Besides there are more inclusions in these specimens (14 for C1, 12 for C2 and 13 for C3) than the ones from the first scenario (Figure 18) and they are evenly distributed within the volumes. These reasons lead to the fact that we see almost no dispersion neither in the axial nor in the volumetric strain measurements : we are addressing an equivalent homogeneous material. Consequently in similar cases, we can safely adjust a phenomenological model and use the resulting parameter set for the concerned underground facility.

To illustrate this, we use the same constitutive model introduced in section 3 to fit the curve C1 in Figure 21. We assume that the stress and strain fields within the specimen are homogeneous, all the stresses are compressive and therefore the tensile mechanism cannot be activated. We set $z \neq 0$ in order to reproduce the volumetric strain. In other words, the results shown in Figure 21 for the specimen C1, are considered experimental data to fit with the the proposed model under the assumptions stated. Figure 22 shows the fitting of these data with the parameter set given in Table 3. As it can be seen, the phenomenological model, where dilatancy is taken into account on a constitutive level, matches very well the results.

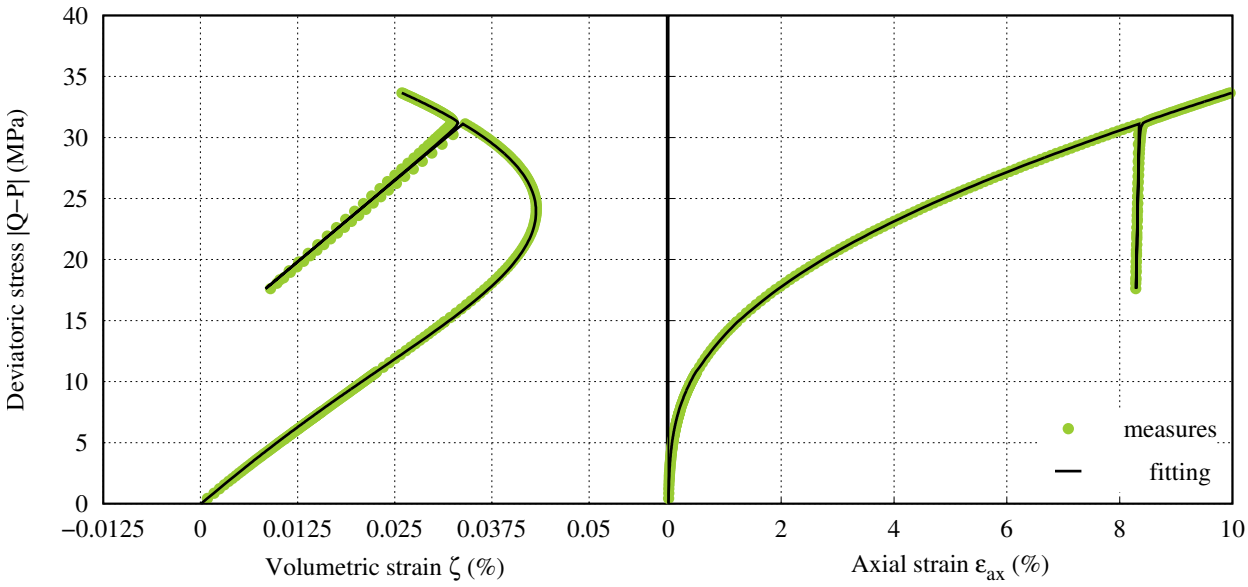

Figure 22: Fitting of a conventional triaxial compression test (P=5 MPa and $\dot{\varepsilon} = 10^{-6}$ s^{-1}) conducted on specimen C1 shown in Figure 20.

Elasticity					
E	ν				
22523	0.29				
Distorsion					
a	k	b	B	K	C
0.21	2.7	0.29	0.03	0.1	0
Dilatancy					
z	n	N	m	M	
1.3	1.07	0.0012	2.05	0.0058	
Tension					
d	Λ	R_t	S	s	
10	0	0	1	1	

Table 3: Parameters used to fit the triaxial test results C1 shown in Figure 21. The unit system is such that strain is in μm/m, stress is in MPa and time in days.

5. Conclusions

In this paper, the volumetric strain measurements were experimentally investigated through the analysis of over 120 typical triaxial compression tests on salt specimens from different locations. The difference between local and global measurements exhibited during this analysis, raised questions concerning the effect of material spatial heterogeneity on the volumetric behavior and consequently on the representativity of the used specimen. We chose to focus on a specific aspect of material heterogeneity: the presence of nodules of insoluble materials within a pure halite matrix, in order to obtain a qualitative understanding of the issue.

We carried out a numerical study during which salt specimens were considered as cylindrical matrices of pure halite with spherical inclusions. We proved that dilatancy can be a consequence of the specimen's material heterogeneity.

We then investigated the experimental observations and proved that the significant differences (in patterns and the measured dilatancy onsets) between local and global volumetric strain measurements, were satisfactorily explained by the material spatial heterogeneity.

Finally, found that the presence of nodules of insoluble materials within a salt rock could lead to representativity issues. And in that case, we propose the following general methodology :

1. Characterize one of the used specimens (known to be not representative): volume fraction of insoluble materials, the nature of the inclusions (thus getting an estimation of their elastic constants), the concentration zones of heterogeneity.

2. Model this specimen as a two-phase medium composed of a pure halite matrix and nodules of insolubles.

3. Perform a history matching of the experimental data with a given constitutive model (in which dilatancy results from the activation of a tensile mechanism induced by the presence of heterogeneities) on the modeled structure.

4. Once a parameter set is obtained, model a representative specimen: containing much more inclusions of a negligible size compared to the dimensions of the specimen.

5. Simulate the test conducted in the lab on the representative specimen using the same constitutive model from step 3 with the parameter set resulting from the history matching.

6. The obtained results are supposed to be representative of the rock in question. They can be fit with a given phenomenological constitutive model assuming the homogeneity of the stress field. Dilatancy in the chosen model should be taken into account on a constitutive level. The resulting parameter set can then be used for the corresponding rock salt.

This methodology combines experimental work with numerical modeling in order to overcome specimens representativity issues and the limitations of laboratory testing procedures.

Acknowledgments

The authors would like to thank their colleagues Michel Tijani and Faouzi Hadj-Hassen from MINES ParisTech for their valuable contributions.

References

Bays, C. A., 1963. Use of salt cavities for underground storage. In: Symposium on Salt.; Northern Ohio Geological Society. Cleveland, Ohio, pp. 564–578.

Chemin, P., Nov. 1990. Etude du rôle des inclusions fluides dans les mécanismes de déformation des roches halitiques. Application aux formations salifères du bassin bressan. Theses, Ecole Nationale des Ponts et Chaussées.

DeVries, K., Mellegard, K., October 2010. Effect of specimen preconditioning on salt dilation onset. In: SMRI fall 2010 technical conference. Leipzig, Germany.

DeVries, K., Mellegard, K., Callahan, G., Goodman, W., 2005. Cavern roof stability for natural gas storage in bedded salt. Technical report de-fg26-02nt41651, RESPEC, Rapid City, South Dakota.

DeVries, K. L., Mellegard, K. D., Callahan, G. D., 11 2002. Salt damage criterion proof-of-concept research. Technical report rsi-1675 de-fc26-00nt41026, RESPEC, Rapid city, South Dakota.

Gillhaus, A., Crotogino, F., Albes, D., 2006. Compilation and evaluation of bedded salt cavern characteristics important to successful cavern sealing, part 1: Worldwide bedded slat deposits and bedded salt cavern characteristics. 2003-5-smri.solution mining research institute research project report.

Günther, R.-M., Salzer, K., Popp, T., Lüdeling, C., 09 2015. Steady-state creep of rock salt: Improved approaches for lab determination and modelling. Rock Mechanics and Rock Engineering 48.

Habibi, R., 2019. An investigation into design concepts, design methods and stability criteria of salt caverns. Oil Gas Sci. Technol. - Rev. IFP Energies nouvelles 74, 14.

Heusermann, S., Rolfs, O., Schmidt, U., 2003. Nonlinear finite-element analysis of solution mined storage caverns in rock salt using the lubby2 constitutive model. Computers Structures 81 (8), 629 – 638, k.J Bathe 60th Anniversary Issue.

Hou, Z., 2003. Mechanical and hydraulic behavior of rock salt in the excavation disturbed zone around underground facilities. International Journal of Rock Mechanics and Mining Sciences 40 (5), 725 – 738.

Labaune, P., 10 2018. Comportement thermomécanique du sel gemme : Application au dimensionnement des cavités. Ph.D. thesis.

Labaune, P., Rouabhi, A., Tijani, M., Blanco-Martín, L., You, T., Feb 2018. Dilatancy criteria for salt cavern design: A comparison between stress- and strain-based approaches. Rock Mechanics and Rock Engineering 51 (2), 599–611.

Mansouri, H., Prior, D. J., Ajalloeian, R., Elyaszadeh, R., 2019. Deformation and recrystallization mechanisms inferred from microstructures of naturally deformed rock salt from the diapiric stem and surface glaciers of a salt diapir in southern iran. Journal of Structural Geology 121, 10 – 24.

Medina-Cetina, Z., Rechenmacher, A., 01 2009. Influence of boundary conditions, specimen geometry and material heterogeneity on model calibration from triaxial tests. International Journal for Numerical and Analytical Methods in Geomechanics 34, 627–643.

Mellegard, K., Callahan, G., Devries, K. L., 01 2005. Lode angle effects on the deformational properties of natural

rock salt. In: American Rock Mechanics Association.

Munson, D., Dawson, P., 1981. Salt constitutive modeling using mechanism maps. In: First conference on the mechanical behavior of salt. pp. 717–737.

Popp, T., Kern, H., 1998. Ultrasonic wave velocities, gas permeability and porosity in natural and granular rock salt. Physics and Chemistry of the Earth 23 (3), 373 – 378.

Roberts, L. A., Buchholz, S. A., Mellegard, K. D., Düsterloh, U., Nov 2015. Cyclic loading effects on the creep and dilation of salt rock. Rock Mechanics and Rock Engineering 48 (6), 2581–2590.

Rouabhi, A., Labaune, P., Tijani, M., Gatelier, N., Hévin, G., 2019. Phenomenological behavior of rock salt: On the influence of laboratory conditions on the dilatancy onset. Journal of Rock Mechanics and Geotechnical Engineering.

Schulze, O., Popp, T., Kern, H., 2001. Development of damage and permeability in deforming rock salt. Engineering Geology 61 (2), 163 – 180, geosciences and Nuclear Waste Disposal.

Speranza, G., Vona, A., Vinciguerra, S., Romano, C., 2016. Relating natural heterogeneities and rheological properties of rocksalt: New insights from microstructural observations and petrophyisical parameters on messinian halites from the italian peninsula. Tectonophysics 666, 103 – 120.

Stormont, J., 1997. In situ gas permeability measurements to delineate damage in rock salt. International Journal of Rock Mechanics and Mining Sciences 34 (7), 1055 – 1064.

Thiemeyer, N., Habersetzer, J., Peinl, M., Zulauf, G., Hammer, J., 2015. The application of high resolution x-ray computed tomography on naturally deformed rock salt: Multi-scale investigations of the structural inventory. Journal of Structural Geology 77, 92–106.

Thiemeyer, N., Zulauf, G., Mertineit, M., Linckens, J., Pusch, M., Hammer, J., 2016. Microfabrics and 3d grain shape of gorleben rock salt: Constraints on deformation mechanisms and paleodifferential stress. Tectonophysics 676, 1 – 19.

Tijani, M., Apr. 2008. Contribution à l'étude thermomécanique des cavités réalisées par lessivage dans des formations géologiques salines. Habilitation à diriger des recherches, Université Pierre et Marie Curie - Paris VI.

Tijani, M., Vouille, G., Hugout, B., 1983. Le sel gemme en tant que liquide visqueux. In: Le sel gemme en tant que liquide visqueux. Melbourne, Australia, pp. 241–246.

Tsang, C.-F., Bernier, F., Davies, C., 2005. Geohydromechanical processes in the excavation damaged zone in crystalline rock, rock salt, and indurated and plastic clays—in the context of radioactive waste disposal. International Journal of Rock Mechanics and Mining Sciences 42 (1), 109 – 125.

Ulusay, R., Hudson, J., for Rock Mechanics. Commission on Testing Methods, I. S., 2007. The Complete ISRM Suggested Methods for Rock Characterization, Testing and Monitoring: 1974-2006. International Society for Rock Mechanics, Commission on Testing Methods.

Van-Hasselt, B., 12 1991. Évaluation qualitative du rôle de la texture dans le fluage du sel bressan. Ph.D. thesis.

Wang, T., Li, J., Jing, G., Zhang, Q., Yang, C., Daemen, J., 2019. Determination of the maximum allowable gas pressure for an underground gas storage salt cavern – a case study of jintan, china. Journal of Rock Mechanics and Geotechnical Engineering 11 (2), 251 – 262.

Wang, T., Yang, C., Chen, J., Daemen, J., 2018. Geomechanical investigation of roof failure of china's first gas storage salt cavern. Engineering Geology 243, 59 – 69.

Wawersik, W. R., Hannum, D. W., 1980. Mechanical behavior of new mexico rock salt in triaxial compression up to 200c. Journal of Geophysical Research: Solid Earth 85 (B2), 891–900.